# Supporting Information for "Induced Plant Defenses, Host-Pathogen Interactions, and Forest Insect Outbreaks"

Bret D. Elderd, Brian J. Rehill, Kyle Haynes, and Greg Dwyer

August 12, 2013

# 1 Details of Experimental Methods, and Additional Experimental Results

## 1.1 JA Application and Chemical Analyses

We randomly selected eight experimental and eight control red oaks, each a mature tree, in an oak-hickory forest in southwest Michigan, at the Lux Arbor site of the Kellogg Biological Station ($42.4\,^{\circ}\mathrm{N}$, $85.4\,^{\circ}\mathrm{W}$). On each of the 8 experimental trees, we randomly assigned 3 branches to the JA spray, and 3 to the non-JA control spray. We sprayed branches for three weeks, weather permitting, beginning shortly after bud burst. Experimental branches were treated with 5 mM jasmonic acid (JA) initially solubilized in a solution of 10% EtOH (aq., v/v) that also included 0.125% (v/v) Triton-X detergent to permit JA to penetrate leaf cuticles. Control branches were treated with a solution that lacked JA, but that was otherwise identical. In addition to control branches on experimental trees, control branches included three branches on each of 8 control trees on which there were *no* branches sprayed with JA. It turned out, however, that hydrolyzable tannin concentrations in control branches on these latter control trees were indistinguishable from concentrations in control branches on trees on which there *were* JA-sprayed branches (mixed-effects repeated-measures analysis on hydrolyzable tannin concentrations in control branches, with trees, and branches nested within trees, as random effects: $F_{1,46} = 0.81$, $p = 0.3728$). Control branches on JA-sprayed and non-JA-sprayed trees were therefore effectively identical. To quantify changes in hydrolyzable tannin concentrations, we collected samples at budburst, and again 3 weeks later, 24h before the initially uninfected larvae in the experiment began feeding on the branches.

We flash-froze our single-leaf samples in liquid nitrogen, and we kept them on dry ice for roughly two hours until storage at $-80\,^{\circ}\mathrm{C}$. Each sample was then lyophilized, and ground in a mortar and pestle under liquid nitrogen. We next placed 25 mg of each lyophilized, ground sample in a 2 ml microcentrifuge tube, and we extracted it exhaustively by sonication for 2 hours with a total of 2 ml 70% (v/v) acetone at $4\,^{\circ}\mathrm{C}$. We then removed the acetone using rotary evaporation, and we used the aqueous extract in phenolic assays, as follows. We quantified hydrolyzable tannins using the potassium iodate method (Bate-Smith 1975; Schultz and Baldwin 1982), and condensed tannins (proanthocyanidins) using the n-butanol/HCL method (Bate-Smith 1975). Concentrations for each

class of compound were calculated based on standard curves generated with oak tannins purified by a modification of the method of Hagerman and Butler (1980).

## 1.2 Results from Sample Collections in the Year Following JA Spray

Previous work showed that defoliation of red oak in one year can lead to hydrolyzable tannin induction in the following year (Hunter and Schultz 1993). We therefore collected a final set of samples from each branch in the season following our experiments, again at budburst. In the year following

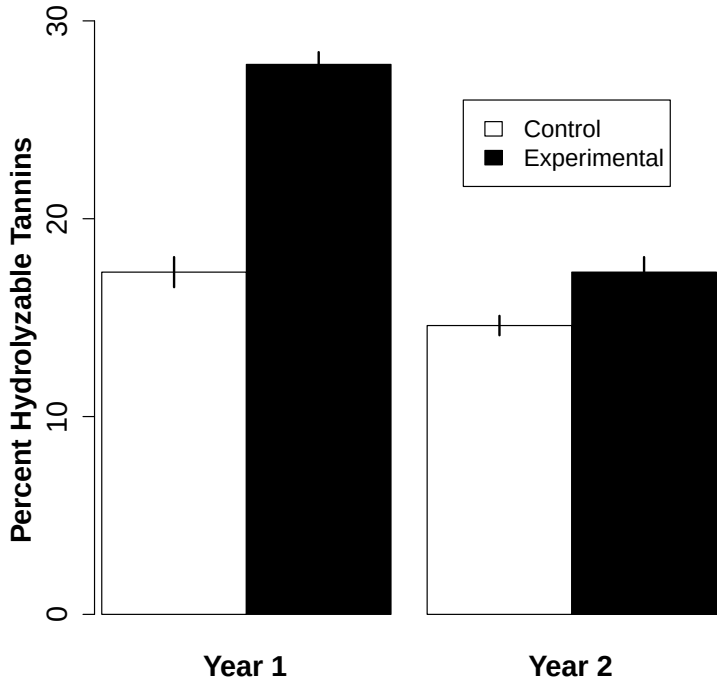


Figure S1: Percent hydrolyzable tannin concentrations in experimental branches. Year 1 is the year in which branches were sprayed, while Year 2 is the following year. Error bars indicate 1 standard error of the mean.

JA application, the average difference between JA-sprayed branches and non-JA-sprayed branches was lower (first year: $8\% \pm 1.16$; second year: $3\% \pm 0.90$), but it was again significant (fig. S1, $F_{1,20} = 5.54$, $p = 0.0289$). The effect of JA spray was thus carried over from one year to the next.

## 1.3 Insect Rearing Protocols and Variability in Infection Risk

Key features of our protocol reduced extraneous sources of variability, and previous experiments have shown that the protocol therefore allows for surprisingly high statistical power (Dwyer 1991; Fuller et al. 2012). Following this protocol, we used larvae from a USDA colony of low variability, and a plaque-purified virus strain known as "G2" (Dwyer et al. 2005). Also, to match the timing of key transmission rounds in nature (Woods and Elkinton 1987), we used uninfected larvae that were in the third larval stage or "instar". Finally and most importantly, because susceptibility to the baculovirus changes over a period of hours after molting (Grove and Hoover 2007), we ensured that the uninfected larvae were developmentally synchronized, using the following procedure.

Because we wanted to use third instars, from the larval rearing cups we collected second instars whose head capsules had slipped forward, which indicates that molting to the next instar will occur within 24 hours. As we collected these larvae, we held them at $4\,^{\circ}\mathrm{C}$ in a cold room until we had collected enough of them to carry out the experiment, which took roughly 48 hours. We then removed the larvae from the cold room, and held them in cups without diet at $25\,^{\circ}\mathrm{C}$ for another 48h, by which time essentially all of them had molted to the third instar. In practice, almost all molting occurred within the first 24h at $25\,^{\circ}\mathrm{C}$, ensuring a high degree of developmental synchrony. Because larvae stop feeding once their head capsules slip forward, using recently molted larvae had the additional advantage that it minimized the effects of previously consumed food items, a crucial issue in studies of the effects of diet on insect infection risk (Keating et al. 1989).

We produced infected larvae by feeding virus-contaminated diet to neonates, using a dose high enough to ensure more than 95% infection. To be certain that that the infected larvae were indeed infected, we held them at $26\,^{\circ}\mathrm{C}$ for five days, a period long enough to ensure that any uninfected larvae would molt to the second instar, which allowed us to identify and discard the uninfected larvae. We then placed the infected larvae on branches in the field five days before adding uninfected larvae, which is long enough to ensure that the infected larvae would distribute themselves naturally over the branches before dying. Densities of healthy and infected larvae were chosen to match densities in nature (Woods and Elkinton 1987). All larvae were enclosed in mesh bags, which do not affect foliage chemistry or larval behavior, but prevent the loss of insects to dispersal, and the loss of virus to UV degradation, while allowing for natural variability in weather conditions (Fuller

et al. 2012).

The initially uninfected larvae began feeding after leaves were fully expanded, which is when leaf chemistry ceases to change, so defoliation during the field experiment had no effect on hydrolyzable-tannin levels (D'Amico et al. 1998). Meanwhile, 25 uninfected larvae is a large enough number to provide reasonable statistical power, but it prevents starvation because 25 larvae per 40 leaves leads to defoliation levels of less than 50%. We further note that the density of initially uninfected larvae during a field transmission experiment has little to no effect on infection rates or induced defenses (D'Amico et al. 1998).

As in previous experiments (Dwyer et al. 2005), our protocol did not eliminate the effects of variability in infection risk, raising the question, what is the source of the variability? The answer is almost certainly *not* stochastic fluctuations in infection risk within individuals over time, because such variability is equivalent to demographic stochasticity, and by using hundreds of insects, we greatly reduced the effects of demographic stochasticity. Instead the source appears to be heritable variation at loci that affect infection risk. In previous work, we showed that infection risk in gypsy moth larvae does indeed have a heritable component (Elderd et al. 2008), and because the larvae in the current study were all raised under the same conditions, the variability that we observed here was also probably heritable. In gypsy moths, heritable variation in infection risk is likely maintained by fluctuating natural selection, in combination with a fecundity cost of resistance (Elderd et al. 2008). We did not include selection in our models, however, because we wanted to explain the defoliation data with as simple a model as possible.

## 1.4 Analysis of Transmission Data

Because virus density was constant in our field experiment, and because the experiment was short enough that none of the initially uninfected larvae became infected and died during transmission, infection was the only process that occurred. This in turn meant that we could analyze our data using what is known in the stochastic processes literature as a "pure-death" model, which allows for the effects of small population size, so-called "demographic stochasticity" (Renshaw 1993). Because we used a total of 200 host insects in each experimental treatment (8 replicates $\times$ 25 larvae per replicate), the effects of demographic stochasticity were likely minimal, but it was nevertheless

important to allow for such effects (Dwyer et al. 2005; Elderd et al. 2008). The pure-death process predicts that the number of survivors per unit time follows a binomial distribution with a probability of survival that is a function of time and a rate parameter that can be fit to the data (Renshaw 1993). Also, because individuals vary in their risk of infection, we assume that the pure-death parameter, which is essentially the disease transmission rate, is drawn from a gamma distribution, with mean transmission rate $\bar{\nu}$ and coefficient of variation $C$.

Standard practice in analyzing mortality data is therefore to use a binomial distribution as a likelihood function McCullagh and Nelder (1989), and we thus used a binomial likelihood function in our analyses. Given the likelihood function, the $\text{AIC}_c$ is calculated according to:

$$\text{AIC}_c = -2L + 2K\left(\frac{n}{n-K-1}\right). \tag{S1}$$

Here $L$ is the likelihood of a given model, $K$ is the number of parameters in the model, $n$ is the number of replicates, and the term $n/(n-K-1)$ is the correction for sample size. The $\text{AIC}_c$ thus chooses the best-fit model based on a tradeoff between model complexity, in terms of the number of parameters, and goodness of fit, as measured by the likelihood, such that the best model has the smallest $\text{AIC}_c$. In practice, we use $\Delta\text{AIC}_c$ scores to measure the difference in $\text{AIC}_c$ values between the best-fit model and all other models under consideration. The best-fit model thus has a $\Delta\text{AIC}_c$ score of zero. Meanwhile, to calculate the probability that each model is actually the best model, we used $\text{AIC}_c$ weights, which are calculated as:

$$w_i = \frac{\exp\left(-\frac{1}{2}\Delta_i\right)}{\sum_{r=1}^{R}\exp\left(-\frac{1}{2}\Delta_r\right)}. \tag{S2}$$

Here $w_i$ is the weight for the $i$th model, while $\Delta_i$ is the $\text{AIC}_c$ difference for the $i$th model. Relative to traditional significance tests, an advantage of the $\text{AIC}_c$ is that it does not assume that any model being fit to the data is absolutely correct (Burnham and Anderson 2002). This is a crucial advantage, because our goal was to identify the model that best describes our data, but transmission is so complicated that it is unlikely that *any* model could capture every mechanism that might affect transmission.

Preliminary analyses showed that the best models did not distinguish between non-JA-treated branches on non-JA-treated trees and non-JA-treated branches on JA-treated trees, and so we only show analyses in which the two types of branches were treated identically. Moreover, because the

variance-inflation factor was very close to the ideal value of 1, our choice of a binomial distribution was clearly appropriate (Burnham and Anderson 2002). The best model thus explained essentially all of the variability in our data that was not simply due to low levels of demographic stochasticity.

An important point is that allowing variability $C$ to approach 0 in a nonlinear transmission model yields a linear transmission model, and so the linear models were nested within the nonlinear models. This in turn meant that, when we fit a nonlinear transmission model to our data, it was possible for the best-fitting value of the variability parameter to be indistinguishable from 0, in which case the conclusion would be that the best-fitting model is instead linear. This happened for the models for which average transmission was the same for induced and control branches but variability was different, and for which both average transmission and variability were different for induced and control branches. In both of these cases, however, the best-fitting model assumed that transmission was linear *only* on induced branches, and *not* on control branches, strengthening our basic conclusion. Because the best-fitting versions of these two models reduced to simpler models, we did not include them in the AIC table in the main text.

It is also important to emphasize that when we fit a *linear* model to the data, the fitting routine *cannot* estimate the variability parameter, and so in such cases it would not be possible for the routine to conclude that the best model is nonlinear. This is relevant because when we fit a model for which transmission was nonlinear for induced branches and linear for control branches, the fitting routine instead concluded that transmission was linear for both treatments. In the AIC table in the main text, we therefore did not include the model that assumed transmission was nonlinear on induced branches and linear on control branches, because it was effectively the same as the model for which transmission was assumed, from the beginning, to be linear for both treatments. As the table shows, however, the model for which transmission was linear for both treatments provided a very poor explanation for the data, again strengthening our basic conclusion.

An important part of our argument is that induction strongly affects variability $C$ in particular. This conclusion is supported by our parameter estimates for the best model, which allows for differences in both average infection risk $\bar{\nu}$ and variability in infection risk $C$ between induced and control branches. As Table S1 shows, the value of $\bar{\nu}$ on induced branches was moderately lower, reflecting slightly lower average infection risk on induced branches, as in a previous laboratory experiment (Hunter and Schultz 1993), but the value of $C$ was *much* lower, reflecting much lower variability in

| Experiment | Treatment | Mean (95% C.I.) | C.V. (95% C.I.) |
|---|---|---|---|
| Field | Control | $0.21$ /day/m$^2$ $(0.170, 0.276)$ | $0.96$ $(0.741, 1.177)$ |
| | Induced | $0.12$ /day/m$^2$ $(0.111, 0.136)$ | $0$ $(0, 0.458)$ |
| Laboratory | Control | $3.19$ $(2.725, 3.654)$ | $0.17$ $(0.076, 0.264)$ |
| | Induced | $3.90$ $(3.773, 4.027)$ | $0.09$ $(0.013, 0.167)$ |

Table S1: Effects of induction on parameters describing infection risk (the protocol for the laboratory experiment is given in a later sub-section). For the laboratory experiment, the mean is the $\log_{10}$ of the 50% lethal dose, or "$LD_{50}$", the number of occlusion bodies required to cause 50% mortality, which is an *inverse* measure of infection risk. A lower $LD_{50}$ is thus equivalent to a higher average infection risk. For the field experiment, the mean is the average transmission rate $\bar{\nu}$, the probability of infection per unit time and per infectious cadaver per square meter, while the C.V. is the parameter $C$, the variability in infection risk.

infection risk. Both effects were statistically significant, in that the corresponding 95% confidence intervals for both $\bar{\nu}$ and $C$ for induced branches did not overlap with the 95% confidence intervals for non-induced branches. Also, although Table S1 shows that the best estimate of $C$ on induced foliage was 0, this does not mean that variability in infection was truly 0 on induced foliage. Instead it was simply too low for its effects to be detectable in our experiment.

To see the consequences of these parameter estimates for baculovirus epizootics, we inserted our best-fit values of transmission $\bar{\nu}$ and variability $C$ for induced and non-induced foliage into the epizootic model equations in the main text. Fig. S2 then shows that the lower value of transmission $\bar{\nu}$ on induced foliage modestly raises the lowest density at which virus epizootics occur, but the lower value of variability in transmission $C$ causes the infection rate to increase much more sharply with host density.

As we mentioned in the main text, this figure resolves an important conundrum associated with Hunter and Schultz (1993)'s previous laboratory experiment, which detected only a reduction in average risk. Induction in nature occurs in response to severe defoliation, which in turn becomes more likely as host densities increase. If induction acted only to reduce average infection risk, then infection rates would fall with increasing host density (Hunter and Schultz 1993), following so-

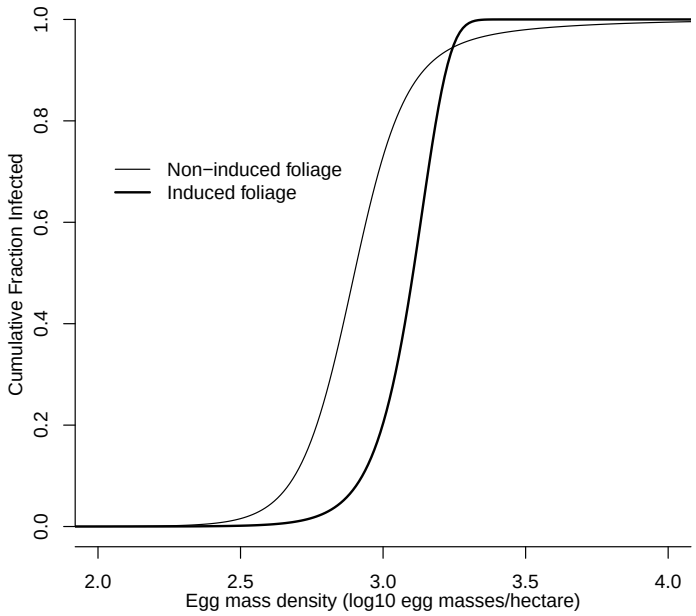


Figure S2: Effects of induction on epizootic intensity. The vertical axis is the cumulative fraction infected in a single epizootic, as calculated using the epizootic model in the main text. The "Induced" line is based on values of average transmission $\bar{\nu}$ and variability in transmission $C$ estimated from induced foliage, while the "Non-induced" line is based on values estimated from non-induced foliage.

called "negative" density-dependence, but baculovirus infection rates in nature almost invariably rise with increasing host density, following "positive" density-dependence (Moreau et al. 2005; Woods and Elkinton 1987). Meanwhile, fig. S2 shows that a reduction in variability in infection risk causes the infection rate to rise more steeply with host density, which is a well-known result from epidemic theory (Anderson and May 1991). Theory therefore shows that a reduction in variability in infection risk due to induction should cause infection rates to rise very sharply with density, resolving the contradiction between the original experiment and data from naturally occurring virus epizootics in the field.

## 1.5 Feeding Trials and Dose-Response Bioassays

Once an insect has consumed some virus particles, infection risk depends only on the ability of the insect's immune response to fight off the infection, but feeding behavior can alter the risk that the virus is consumed in the first place. In dose-response experiments, however, insects that do not consume the entire dose are discarded, and so infection rates depend only on the insect immune response, or on physiological factors that affect the immune response (Watanabe 1987). There are thus no effects of feeding behavior, even though feeding behavior is important in nature (Dwyer et al. 2005). Field transmission experiments thus have an advantage over laboratory dose-response experiments not just because field experiments allow for more natural conditions, but also because they allow for effects of both host behavior and host immune responses on transmission.

Dose-response experiments are nevertheless useful because they allow us to measure the effects of induction of induced defenses on immunological or physiological susceptibility independently of any effects on feeding behavior. Meanwhile, by directly measuring foliage consumption rates, we can measure the effects of induction on feeding behavior in the absence of any effects on immunological susceptibility. Previous work in the fourth author's lab has therefore shown that such a combination of field transmission experiments, laboratory dose-response experiments, and laboratory feeding-rate experiments can be used to understand how immunological susceptibility and host behavior combine to determine infection risk in the field (Dwyer et al. 2005).

To explain our dose-response and feeding experiments, it is useful to think of the overall risk of infection in terms of simple probability (Dwyer et al. 2005), with $P(I, C)$ as the probability of

consuming the virus and becoming infected, $P(I|C)$ as the probability of becoming infected given that the virus has been consumed, and $P(C)$ as the probability of consuming the virus. Following basic probability (Ross 1984), we can then write,

$$P(I, C) \;=\; P(I|C)P(C). \tag{S3}$$

We interpret this equation to mean that the overall probability of infection $P(I, C)$ depends on both immunological susceptibility, as measured by $P(I|C)$, and exposure risk, as measured by $P(C)$.

The goal of our dose-response and feeding experiments was therefore to disentangle the effects of induction on the probability of consumption from the effects of induction on the probability of infection given consumption. Ideally, we would have liked to measure both indices in the field, but such experiments have proved to be impractical. A laboratory dose-response experiment therefore provided a measure of the probability of infection given virus consumption $P(I|C)$, while a laboratory feeding experiment provided a measure of an important determinant of the probability of consumption $P(C)$.

To ensure that the composition of foliage in our dose-response and feeding experiments was as close as possible to the composition of the foliage in the field, the two laboratory experiments were carried out within 24 hours of when uninfected larvae first began feeding in our field transmission experiment, and in both experiments we used leaves from the same branches as in the transmission experiment. To further ensure the validity of comparisons between the field and laboratory experiments, we used the same strain of the insects and the same strain of the virus in all experiments.

In the feeding experiment, we fed single leaves to each of 116 larvae in individual cups, such that 56 larvae were fed leaves from experimental branches and 60 were fed leaves from control branches. Before the experiment began, we measured the area of the leaves using a leaf-area meter, and we re-measured the leaves after the larvae had fed on them for 24 hours. The reduction in area after 24 hours is thus a measure of feeding rate. As fig. S3 shows, feeding rates were substantially higher on induced foliage than on non-induced foliage. We analyzed these data using a mixed-effects generalized linear model (Pinheiro and Bates 2004), as in the hydrolyzable-tannin analysis, such that branches were treated as random effects, nested within a tree, and the JA treatment was the fixed effect. This analysis revealed a significant effect of JA treatment on amount of foliage consumed ($F_{1,118} = 11.48$, $p = 0.001$). We thus conclude that induction of hydrolyzable tannins

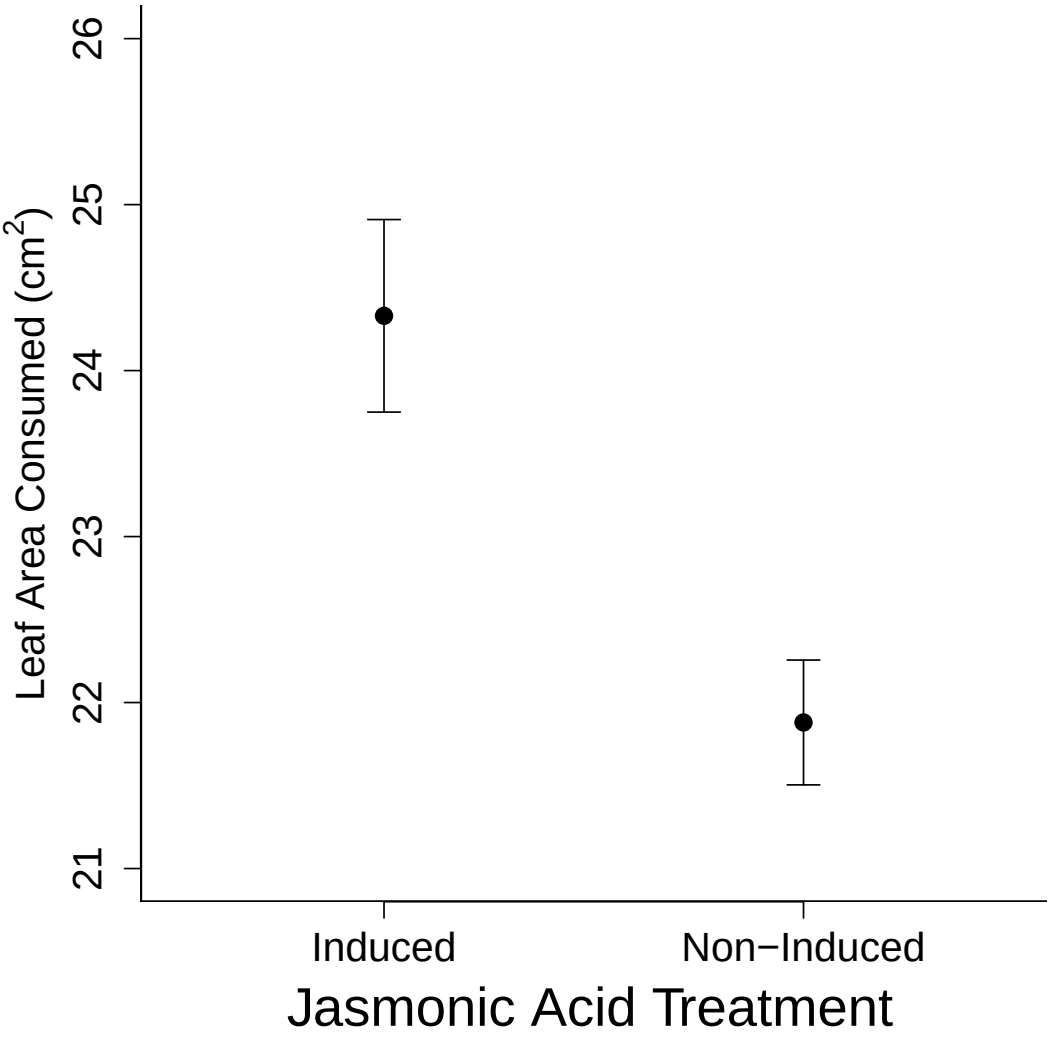


Figure S3: Effects of induction on gypsy moth feeding rate over 24 hours. Error bars indicate 1 standard error of the mean.

leads to increases in feeding rates, in turn altering infection risk. It therefore seems likely that the effects of induction on overall transmission were partly due to changes in feeding behavior.

In the dose-response experiment, we followed standard protocols by feeding larvae 3 $\mu$l of a solution of virus in $dH_2O$ on leaf disks placed on top of agar squares in tightly sealed plastic cups in the laboratory (Dwyer et al. 2005; Hunter and Schultz 1993). Larvae that did not consume the entire leaf disk, and thus the entire dose of virus, were discarded. Control larvae were fed leaf disks with $dH_2O$ alone. The data show that induction led to a lower infection rate at the lower dose, but infection rates were equal at the higher dose (Table S2).

| | Dose (occlusion bodies) | | |
|---|---|---|---|
| Treatment | 0 | 9,000 | 30,000 |
| Induced | $0.00 \pm 0.000$ | $0.56 \pm 0.109$ | $0.97 \pm 0.017$ |
| Non-Induced | $0.00 \pm 0.000$ | $0.86 \pm 0.050$ | $0.97 \pm 0.032$ |

Table S2: Results of the dose-response bioassay, comparing the effects of induced and non-induced foliage on the probability of becoming infected given consumption of a particular dose of virus. Each value is the mean fraction infected, calculated across 6 replicates, plus or minus 1 standard error of the mean. Within a replicate, leaf disks were all from the same tree. Each replicate included 11-14 larvae. Out of 250 individuals in virus-control treatments, all of which were fed leaf disks in combination with $dH_2O$, none became infected.

The standard method of analyzing this type of data is to use generalized linear modeling to fit a logistic distribution to the data, using the so-called "logit transform" (Collett 2003). Under this transform, our model for the dose-response data is,

$$\log\left(\frac{1-p_i}{p_i}\right) \;=\; \beta_0 + \beta_1 \log_{10} D_i. \tag{S4}$$

Here, $p_i$ is the fraction infected at dose $D_i$, and $\beta_0$ and $\beta_1$ are parameters that are fit to the data. We fit versions of this model to the data under different assumptions about the effects of induction on the model parameters $\beta_0$ and $\beta_1$. If there were effects of induction, then in the best model either $\beta_0$ or $\beta_1$ or both would differ between the experimental and control treatments. Our statistical approach was therefore to calculate a likelihood score for each version of the model, which we then used

Table S3: AIC analysis of bioassay data. The best model is in bold-face.

| Model | $AIC_c$ | $\Delta$ $AIC_c$ | $AIC_c$ weights |
|---|---|---|---|
| No effect of dose or induction | 283.47 | 27.92 | 0.000 |
| Induction affects only $\beta_0$ | 257.46 | 1.90 | 0.242 |
| Induction affects only $\beta_1$ | 258.68 | 3.12 | 0.132 |
| **Induction affects both $\beta_0$ and $\beta_1$** | 255.56 | **0.00** | **0.626** |

to calculate the $AIC_c$. To do this, we used a generalized, linear, mixed-model fitting routine for binomial data (Collett 2003) assuming quasi-binomial error, with tree as a random effect.

As Table S3 shows, the best model assumes that induction affects both $\beta_0$ and $\beta_1$. Moreover, there was essentially zero probability that the best model was the model that assumed that there was no effect of induction. The dose-response experiment thus showed that part of the reason why induction affected infection risk in the field was because it affected immunological susceptibility. We note, however, that the data do not clearly distinguish between the model that assumes that induction affects both model parameters, and the models that assume that it affects either $\beta_0$ alone or $\beta_1$ alone. For our purposes, however, the important point is that there was an effect of induction on immunological susceptibility.

Because we are interested in the effects of induction on variability in infection risk, we also went beyond standard logit analyses to consider what our data tell us about the underlying distribution of susceptibility. In logit analyses, the probability of infection $p_i$ is described by the cumulative distribution function of a logistic distribution. Like most probability distributions, the logistic distribution has both a mean and a C.V., such that the mean is the $LD_{50}$, the dose that causes 50% mortality. In terms of the parameters $\beta_0$ and $\beta_1$ of the logit equation (S4), the $LD_{50}$ can be expressed as (Evans et al. 1993):

$$LD_{50} = -\beta_0/\beta_1, \tag{S5}$$

while the C.V. can be expressed as:

$$CV = -\frac{1}{\beta_0}\frac{\pi}{\sqrt{3}}. \tag{S6}$$

Given estimates of $\beta_0$ and $\beta_1$, we used the above expressions to calculate the point estimates of the $LD_{50}$ and the C.V. in Table S1. To calculate 95% confidence intervals, we first used the delta method

to calculate standard errors, and then we multiplied the standard errors by 1.96 (Faraway 2006). As the table shows, both average infection risk, as measured inversely by the $LD_{50}$, and variability in infection risk were lower on induced foliaged than on non-induced foliage, matching the field transmission experiment. These differences, however, were only significant for average infection risk, and the difference in C.V.'s was much smaller than in the field transmission experiment. Because field transmission experiments allow for transmission under more natural conditions, however, we do not expect exact agreement between the dose-response experiment and the field-transmission experiment, and in general we place more weight on the results of the field experiment. Our overall conclusion is thus simply that induction affected infection rates in the dose-response experiment, in ways that appear similar to how induction affected infection rates in the field transmission experiment.

# 2 Details of the Models

## 2.1 Type III Predation and Long-term Virus Survival

The Type III functional response in our multi-generation models assumes that the generalist predator switches to gypsy moths as densities increase, but that eventually densities are too high for the generalist to maintain the population at the low-density equilibrium. This assumption is useful because it allows the model to easily mimic the multiple generations of low host densities typically seen in inter-outbreak populations (Dwyer et al. 2004; Elkinton et al. 1996). Moreover, in predator-exclusion experiments, gypsy moth populations show sharp rises in population growth (Jones et al. 1998), suggesting that generalist predators can maintain gypsy moth populations at a low, stable equilibrium, as predicted by Type III models (Dwyer et al. 2004). The term $2abN_n/(b^2 + N_n^2)$ in the model is then the fraction of gypsy moth larvae that are killed by the generalist predators, so that $a$ is the maximum fraction of hosts killed, and $b$ is the density at which this fraction is maximized.

Another important feature of the outbreak model is that it allows for long-term virus survival through both contamination of egg masses and environmental reservoirs. The importance of these mechanisms has been confirmed by extensive field experiments using the gypsy moth and its baculovirus (Murray and Elkinton 1989; Podgwaite et al. 1979). For baculoviruses of other insects,

however, similar field experiments have not been carried out, and apparently as a consequence the literature on baculoviruses often invokes virus survival through covert infections, which are assumed to be activated by stress at some time after infection, due to unidentified stressors (Il'inykh and Ul'yanova 2005). Although covert infections have in fact been detected in some species of insects (Burden et al. 2003), whether or not such infections play a role in transmission in the field is debatable (see Fuller et al. (2012) for a brief review). Moreover, for gypsy moths in particular, surface-disinfection of egg masses, which we used in all of our experiments, is extremely effective at eliminating vertical transmission (Doane 1969), as it is in many other insects (Kukan 1999). For this reason, reports of vertical transmission through the activation of covert infections can often be more parsimoniously explained by a lack of surface-disinfection (Myers et al. 2000). It therefore seems likely that covert infections play only a small role in virus survival in the gypsy moth, and possibly in many other insects as well. In our model, we thus included only environmental reservoirs and surface contamination of egg masses as mechanisms of virus survival between host generations.

It is nevertheless worth pointing out that in fact our model may be adequate to describe the effects of covert infections as well. The crucial assumption is simply that some fraction of infections from previous generations leads to new infections in the current generation. As long as this fraction does not vary with insect density, and as along as such infections are either rare or occur mostly at the beginning of the larval season, our model may provide an accurate description of the effects of covert infections.

## 2.2 Re-scaling and Estimating Model Parameters

As we mentioned in the main text, we used the temporal model to develop a preliminary understanding of the effects of induction on insect outbreaks, and to generate preliminary estimates of some parameters. Before fitting model parameters to data, however, it was important to identify parameters that have identical effects on the model's predictions, as the values of such parameters will be perfectly correlated and thus statistically non-identifiable. We therefore first re-scaled the model. Because the infection rate depends on the epidemic model in the main text, we re-scaled both the year-to-year state variables $N_n$, $Z_n$, and $D_n$, and the epidemic state variables $S(t)$, $E_i(t)$, and $I(t)$,

as follows:

$$\hat{S}(t) \equiv \bar{\nu}\, S(t), \tag{S7}$$

$$\hat{E}_i(t) \equiv \bar{\nu}\, E_i(t), \tag{S8}$$

$$\hat{P}(t) \equiv \bar{\nu}\, P(t), \tag{S9}$$

$$\hat{N}_n \equiv \bar{\nu}\, N_n, \tag{S10}$$

$$\hat{Z}_n \equiv \bar{\nu}\rho\, Z_n, \tag{S11}$$

$$\hat{D}_n \equiv \psi\, D_n. \tag{S12}$$

Allowing for this re-scaling, the epizootic model becomes:

$$\frac{d\hat{S}}{dt} = -\hat{S}\hat{P}\left[\frac{\hat{S}(t)}{\hat{S}(0)}\right]^{C_n^2}, \tag{S13}$$

$$\frac{d\hat{E}_1}{dt} = \hat{S}\hat{P}\left[\frac{\hat{S}(t)}{\hat{S}(0)}\right]^{C_n^2} - m\delta\hat{E}_1, \tag{S14}$$

$$\frac{d\hat{E}_i}{dt} = m\delta\hat{E}_{i-1} - m\delta\hat{E}_i,\ i = 2, \ldots m, \tag{S15}$$

$$\frac{d\hat{P}}{dt} = m\delta\hat{E}_m - \mu\hat{P}. \tag{S16}$$

Note that variability varies from generation to generation because of changes in induced defenses, such that $C_n = C_0 exp\left(-(\hat{D}_n + \hat{D}_0)\right)$. The multi-generation model is then:

$$\hat{N}_{n+1} = \lambda\epsilon_n\hat{N}_n\left(1 - i(\hat{N}_n, \hat{Z}_n, D_n)\right)\left(1 - \frac{2a\hat{b}\hat{N}_n}{(\hat{b}^2 + \hat{N}_n^2)}\right). \tag{S17}$$

$$\hat{Z}_{n+1} = \phi\hat{N}_n i(\hat{N}_n, \hat{Z}_n, \hat{D}_n) + \gamma\hat{Z}_n, \tag{S18}$$

$$\hat{D}_{n+1} = \hat{\alpha}\hat{N}_n\frac{\hat{D}_n}{\hat{\beta} + \hat{D}_n}. \tag{S19}$$

The model dynamics thus depend on ten parameters, namely $\lambda$, $C_0$, $a$, $\gamma$, $\mu$ and the compound parameters $\phi \equiv \Theta\rho$, $\hat{\alpha} \equiv \frac{\alpha\psi}{\bar{\nu}}$, $\hat{\beta} \equiv \frac{\beta}{\psi}$, $\hat{b} \equiv \frac{b}{\bar{\nu}}$, and $\hat{D}_0 \equiv D_0\psi$. Note that we could also eliminate the baseline variability $C_0$, by setting $\hat{D}_0 \equiv \psi D_0 + \log C_0$, but as we will explain, this re-scaling would make it difficult to fit the model parameters to data on tannin concentrations.

Previous work provides estimates of the reproductive rate $\lambda = 74.6$, the maximum predation rate $a = 0.967$, the scaled predation parameter $\hat{b} = 0.14$ (Dwyer et al. 2004) and the virus decay rate

$\mu = 0.39$ /day (Fuller et al. 2012). The parameters $C_0$, $\hat{\alpha}$, $\hat{\beta}$ and $\hat{D_0}$ in contrast are related to the dynamics of hydrolyzable tannins, and consequently have not been previously measured, while the pathogen over-wintering parameters $\phi$ and $\gamma$ are not well known. To produce preliminary estimates of these six parameters, we therefore followed Kendall et al. (1999) in fitting the period and the amplitude of the model cycles to the corresponding values from a combination of our experimental data and observations of gypsy moth populations in nature. This required that we run the model repeatedly to find sets of parameters for which the model output matched the data.

To understand this fitting procedure, note that hydrolyzable tannins can only be measured as a fraction of a sample's dry weight, because the total dry weight of leaf material in the forest is unknown. In fitting the model to the data, we therefore calculated the amplitude of change in the log of the hydrolyzable tannin concentration $\log_{10}(\hat{D}_n + \hat{D}_0)$, so that total dry weight fell out of the calculation as a scaling constant (note that this would not have been true if we had scaled away the baseline variability $C_0$). In our data, the difference in $\log_{10}$ of hydrolyzable tannin concentrations before and after induction was $0.187 \pm 0.028$. Meanwhile, gypsy moth populations cycle with a period of 5-10 years, and with an amplitude of roughly 3-5 orders of magnitude (Williams et al. 1991). We thus searched for values of $\hat{\alpha}$, $\hat{\beta}$, $\hat{D_0}$, $\phi$, and $\gamma$ for which the amplitude of fluctuations in the host population was at least 3 orders of magnitude, the amplitude of fluctuations in the induced defense was within about $0.06$ of $0.187$, and the cycle period was at least 5 years. We then ran the model for 200 generations, discarding the first 50 generations to avoid transients, and we calculated the average amplitude and the period for the remaining 150 generations. To reduce the computational burden, we temporarily eliminated stochasticity by setting the standard deviation of the random variate $\sigma = 0$.

Fig. S4 shows model output for a set of parameter values that met our fitting criteria. As the figure shows, the host population rises to peaks that are terminated by the pathogen, which has a delayed rise that drives the cycles. The induced defense, however, also contributes to the rise in the pathogen population, because of its effect on variability in infection risk. That is, the rise of the defense, in response to the rise of the host, strengthens the delayed density-dependence of the pathogen, allowing cycles to occur. To demonstrate the importance of the induced defense, in fig. S5 we show model output for a lower value of $\hat{\alpha}$, the scaled rate of increase of the induced defense. As the figure shows, this lower rate of induction leads to damped cycles, eliminating outbreaks altogether.

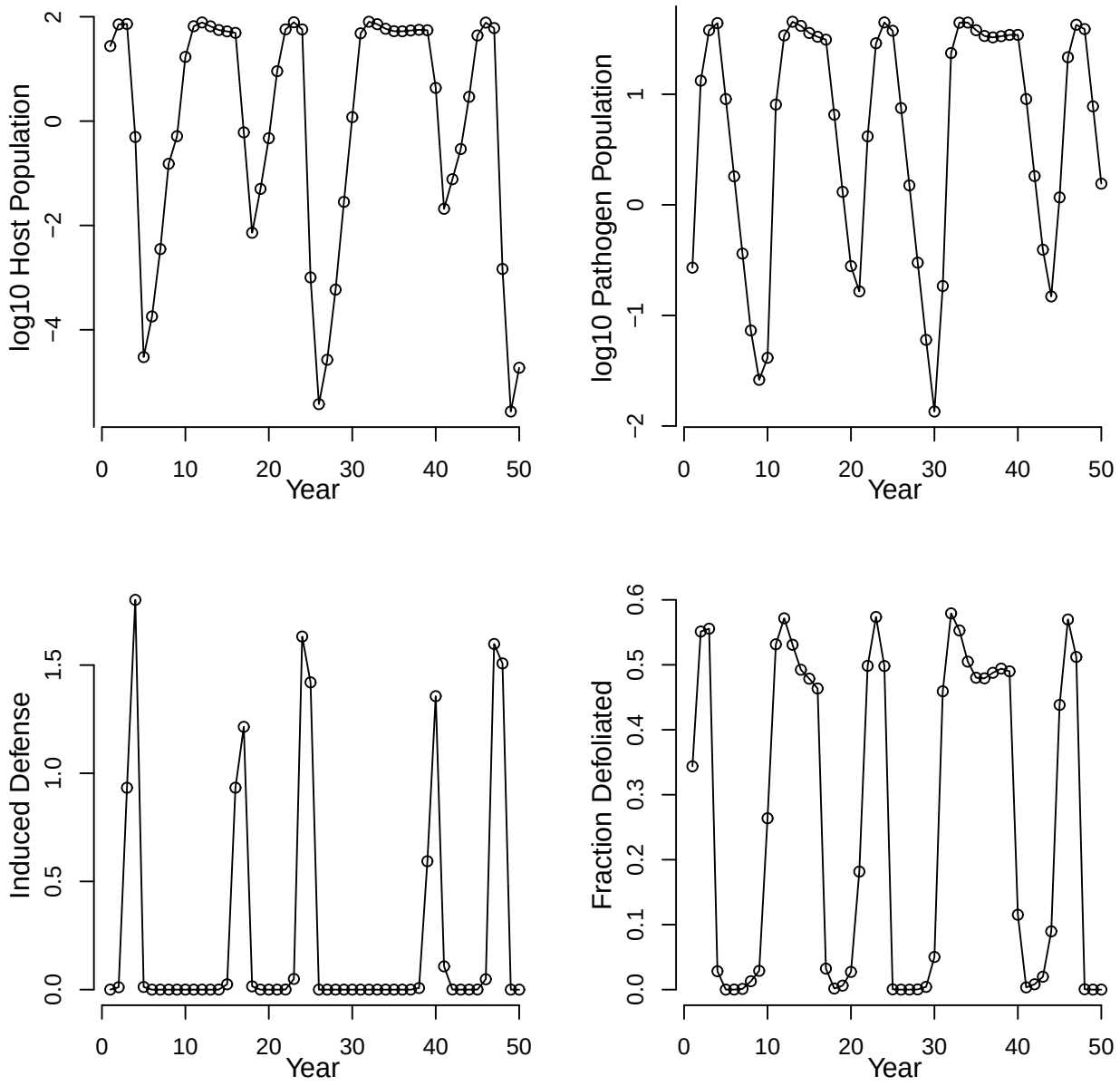


Figure S4: Dynamics of the temporal model. Parameter values are: scaled induction response $\hat{\alpha} = 2.5$, scaled induction half-saturation constant $\hat{\beta} = 100$, baseline heterogenity $C_0 = 0.04$, scaled constitutive defense level $\hat{D}_0 = 3$, long-term virus over-wintering $\gamma = 0.2$, reproductive rate $\lambda = 74.6$, maximum predation rate $a = 0.967$, density at which predation is maximized $b = 0.14$ $\mathrm{m}^{-2}$, virus decay rate $\mu = 0.39$ /day. The average amplitude of the cycles in the induced defense is $0.155$, and the average amplitude of the cycles in the host population is $6.5$ orders of magnitude.

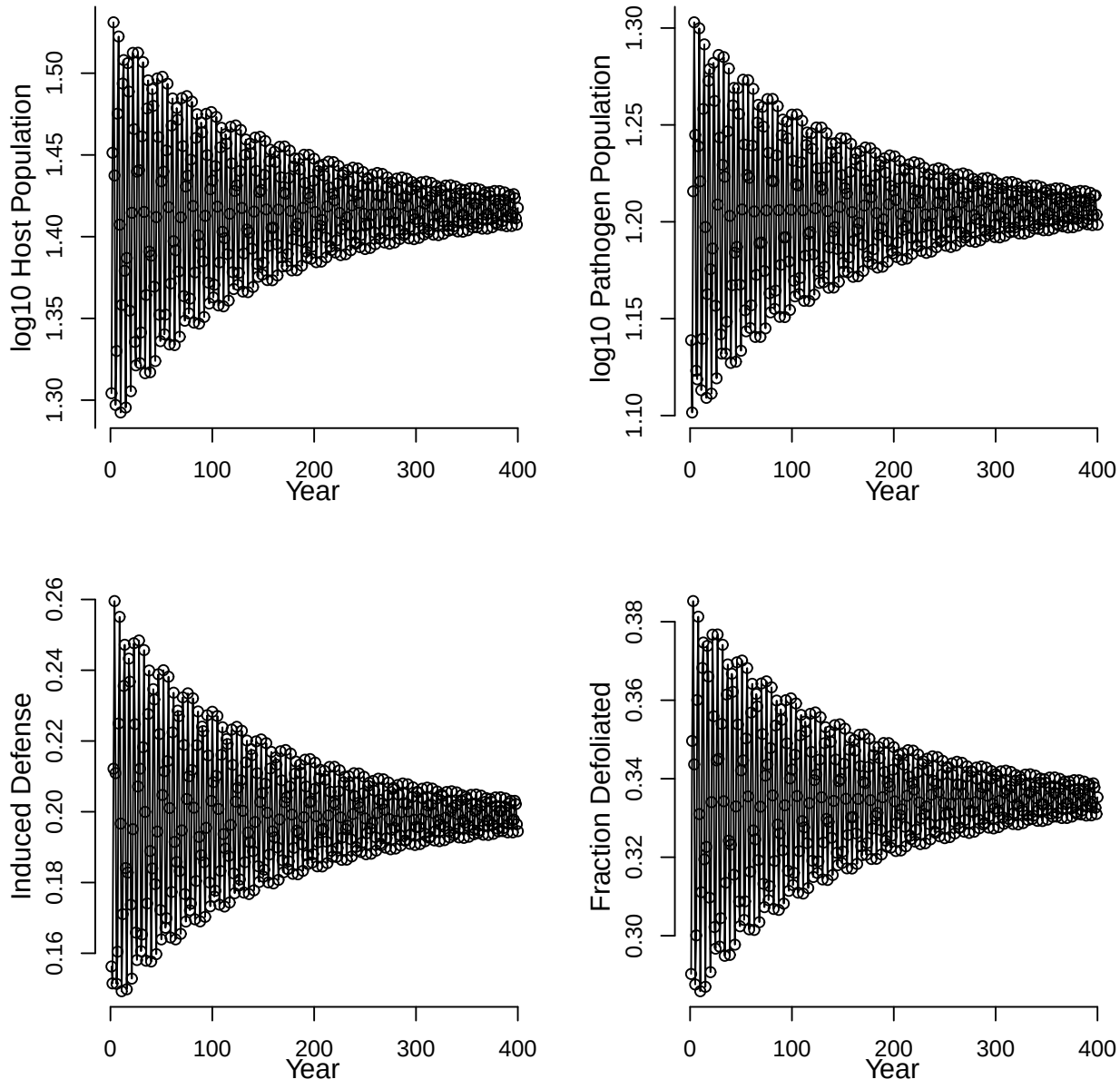


Figure S5: As in fig. S4, except here $\hat{\alpha} = 0.8$, so that increases in the induced defenses are weak. The cycles therefore damp out.

This occurs because, for this value of $\hat{\alpha}$, induction is very weak, so the induced defense never rises high enough to allow for the severe density-dependence that drives outbreaks. The temporal model therefore suggests that induced defenses play a key role in driving gypsy moth outbreaks in nature. The comparison of the spatial model to the defoliation data neverthless provides a more convincing test of the model, and so the spatial model is the focus of the main text.

In figures (S4) and (S5), and in the figures in the main text, we include panels showing fluctuations in the fraction of trees defoliated. To generate those panels, we translated the model prediction of host population density into a fraction defoliated, using a statistical model and associated parameters from the literature, such that the statistical model parameters had been estimated by correlating defoliation levels with egg densities (Williams et al. 1991). Note that, in the non-dimensionalized version of the model, host density is scaled by the average transmission rate $\bar{\nu}$, which in our experiments is expressed in terms of /day/m$^2$ (in the model equations, the m$^2$ unit balances the units on infectious cadavers, which are in terms of /m$^2$). Once we converted from units of m$^2$ to units of acres, we therefore still had $\bar{\nu}$ as a free parameter. The value of this parameter is ultimately of little interest to our results, but for the sake of completeness we note that we achieved a good fit to the oak-hickory defoliation data for a value of $\bar{\nu} = 0.5$ /day/m$^2$, which is well within the 95% confidence interval on this parameter as estimated both from our own data and from previous experiments (Fuller et al. 2012). For oak-pine forests, the best-fit value was a lower value of $\bar{\nu} = 0.1$ /day/m$^2$, which is not surprising given that we expect lower feeding rates, and thus lower infection risk, in forests with a higher fraction of trees that are not oaks.

## 2.3 Details of The Spatial Model

### 2.3.1 Dispersal and Spatial Structure

Because the model is based on a discrete spatial grid, it uses discretized dispersal kernels. For example, for dispersal on automobiles, which is by far the most important type of dispersal Liebhold et al. (1992), the model uses a discretized double-exponential or Laplace distribution Kot et al. (1996):

$$k(d_{q,r}) = \kappa \exp(-\omega d_{q,r}) \; . \tag{S20}$$

Here $d_{q,r}$ is the distance between patch $q$ and patch $r$, such that $\omega$ controls the degree to which dispersal declines with increasing distance from patch $q$ to patch $r$, while $\kappa$ is a scaling constant that ensures that the fraction of individuals dispersing sums to $1$. For dispersal by larval ballooning, we instead used a Gaussian kernel, because it fits the ballooning data better.

Dispersal on automobiles typically occurs when females lay their egg masses on a vehicle. Such egg masses, however, comprise only a small fraction of the total, and so in the model we assumed that a fraction $\zeta$ of each population disperses between patches, after the epizootic, when the egg masses are laid (Liebhold et al. 1992). Based on previous work, we set $\zeta = 10^{-5}$ and $\omega = 0.175$ km$^{-1}$, respectively (Abbott and Dwyer 2008). The transported egg masses then hatch in their new patch the following spring, at which time larvae disperse following a normal dispersal kernel, with an average dispersal distance of $18.9$m, as estimated from data on ballooning larvae (Hunter and Elkinton 2000).

We then set the spatial scale of the model forest to be 25 km on a side, for a total of 625 km$^2$ of forest, a typical forest size in the range of the gypsy moth in North America. We assumed that weather stochasticity was the same across grid cells, ensuring the high level of spatial synchrony typical of gypsy moth populations at this scale Peltonen et al. (2002). Because the defoliation data to which we compared the model were collected in areas that had been colonized by the insect decades earlier Johnson et al. (2006), we assumed that the insect had already infested the entire forest.

At the beginning of each realization of the model, the probability that the tree genera at each location were inducible was determined by drawing a $U(0, 1)$ random variate, such that if this random variate was less than the overall fraction inducible $p$, the location was strongly inducible, otherwise it was weakly inducible. Next, following the way in which the defoliation data were summarized (Johnson et al. 2005), we averaged the fraction defoliated across spatial locations, to produce a single time series of defoliation for each realization of the model. To produce power spectra, we used only the last 50 years of each 100-year simulation, roughly matching the time lag between the introduction of the gypsy moth and when the data were collected, and we averaged the spectra across 100 realizations. Power spectra were calculated using the `spectrum` function in the R programming language (R Development Core Team 2009).

An important point is that power spectra can have minor peaks at integral divisors of the period

associated with a major peak, simply because of the non-sinusoidal character of the data (Chatfield 2003). For our model, however, when the forest is 43% inducible, the peaks of the power spectrum occur at 9 years and about 4.9 years, confirming that the sub-harmonic in the model is not a statistical artifact. The occurrence of non-sinusoidal features in most data sets is also a good reason to combine spectral analysis with visual inspection of the time series being analyzed (Chatfield 2003). In both this document and in the main text, we therefore base our assessment of the fit of the spatial model partly on a visual comparison of model time series to data time series.

As we describe in the main text, individual model realizations vary in the extent to which they reproduce the data, because of stochasticity in forest spatial structure and in the insect's reproductive rate. In figs. S6-S10, we show that, in at least 50% of realizations in oak-hickory forests, there are at least two alternations of high and low outbreaks, as in the data. Moreover, in almost every realization, there is at least one case in which a severe outbreak follows a mild outbreak, or vice versa. In contrast, when the forest is only 15% inducible, corresponding to oak-pine forests, defoliation peaks are *always* moderate, and thus never show the alternation of severe and moderate peaks seen in oak-hickory forests (figs. S11-S15).

An additional detail is that, when we used the parameter values estimated by fitting the non-spatial model in the spatial model, they produced amplitudes of fluctuation that were lower than 3 orders of magnitude, suggesting that spatial structure is stabilizing (for the spatial model, we calculated average amplitudes at each location before averaging across locations, thereby matching how the amplitude data were collected (Williams et al. 1991)). To produce more realistic amplitudes, we first set the standard deviation of the stochasticity to $\sigma = 0.3$ to prevent the model trajectories from being captured by a stable attractor (Dwyer et al. 2004). Second, we increased the scaled growth rate of the induced defense $\hat{\alpha}$ on inducible trees from $\hat{\alpha} = 2.5$ to $\hat{\alpha} = 8$.

Changing $\hat{\alpha}$ also changed the frequency with which the alternation of mild and severe outbreaks occurred in the model. In the realizations shown in figs. S6-S11, we set $\hat{\alpha} = 8$ on inducible foliage, and $\hat{\alpha} = 1$ on non-inducible foliage, which as we described produced at least two alternations in 50% of realizations. Reducing $\hat{\alpha}$ on inducible foliage to 4, however, only reduced the frequency of alternation to about 40%, while reducing it to 2.5 reduced the frequency to about 25%. Likewise, reducing the value of $\hat{\alpha}$ on non-inducible foliage to 0.5 only lowered the frequency of alternation to about 40%, while reducing it to 0.25 lowered the frequency to about 20%. Raising either value of

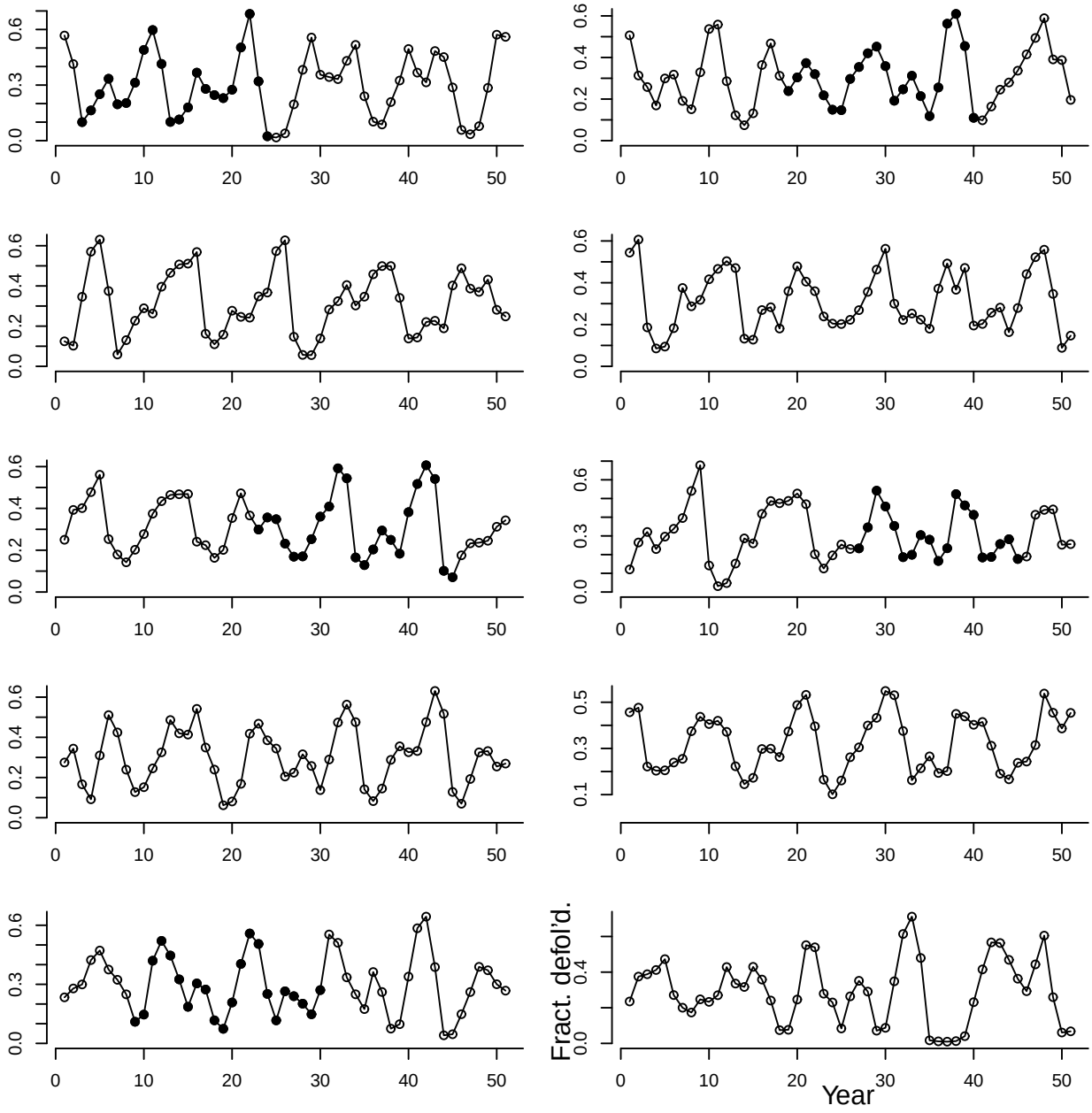


Figure S6: 10 realizations of the spatial model, with 43% of the forest inducible, corresponding to oak-hickory forests. Filled circles identify time periods during which model output provides a near-exact visual match to the defoliation data.

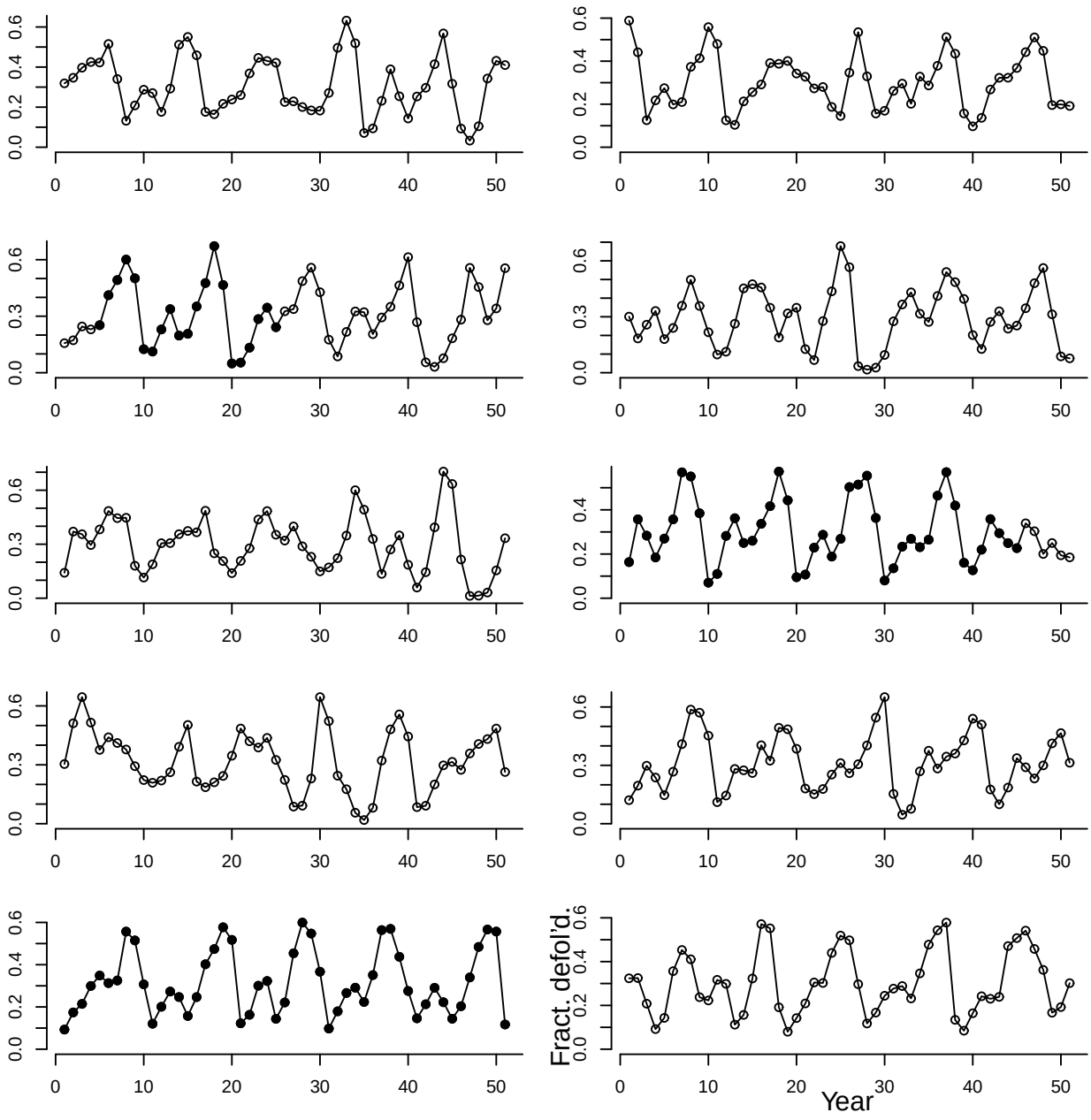


Figure S7: 10 additional realizations of the spatial model, as in fig. S6.

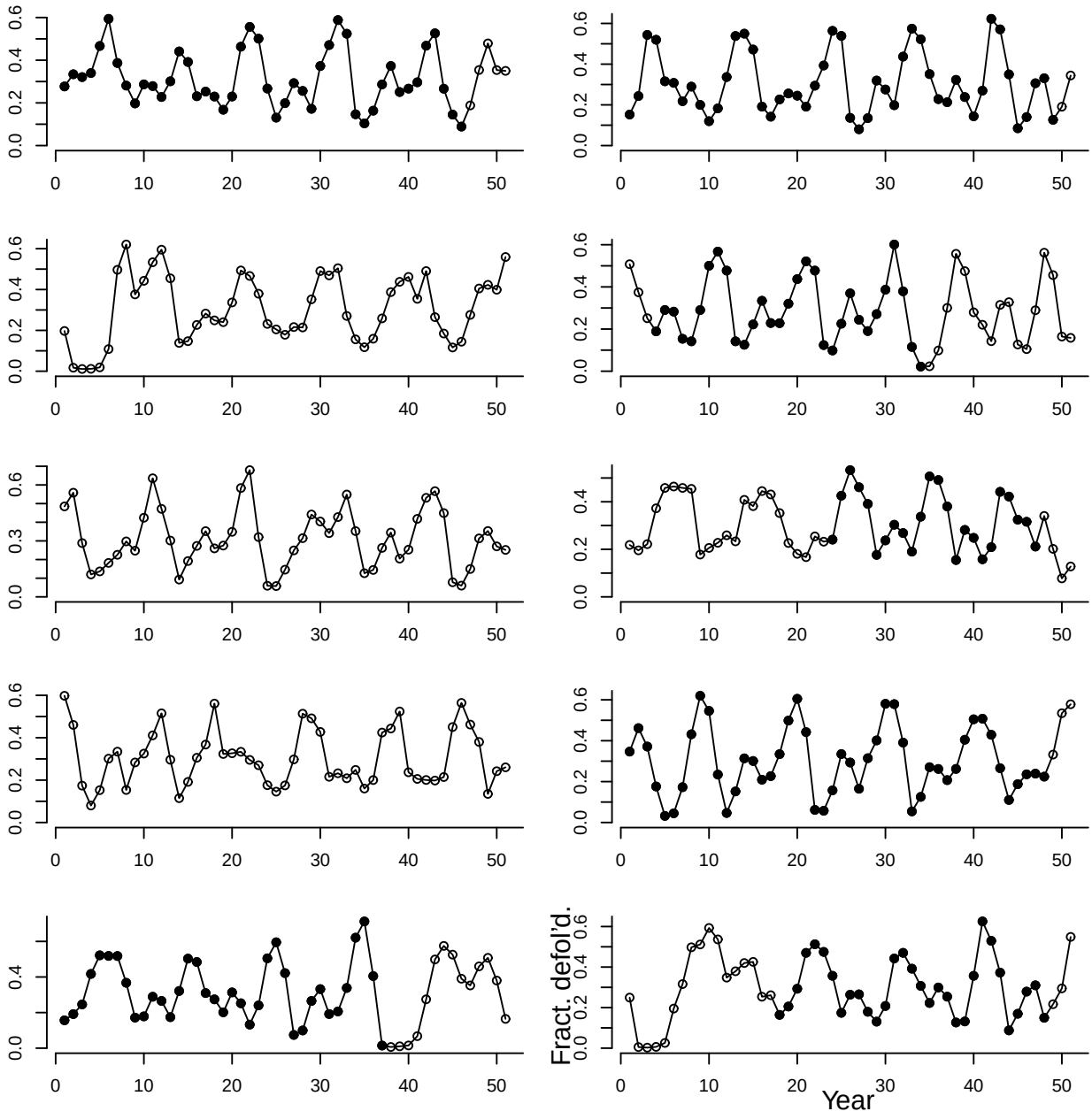


Figure S8: 10 additional realizations of the spatial model, as in fig. S6.

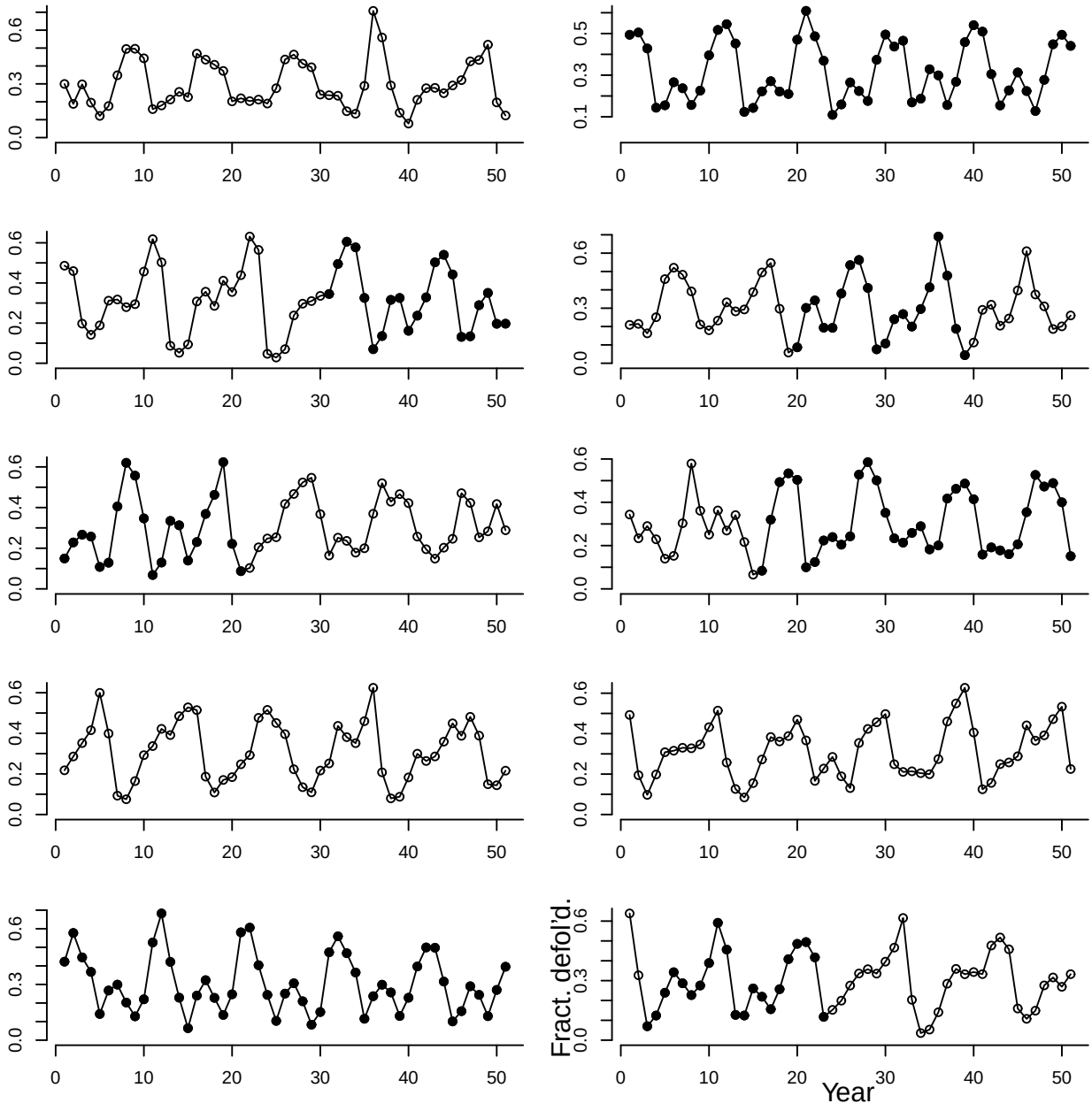


Figure S9: 10 additional realizations of the spatial model, as in fig. S6.

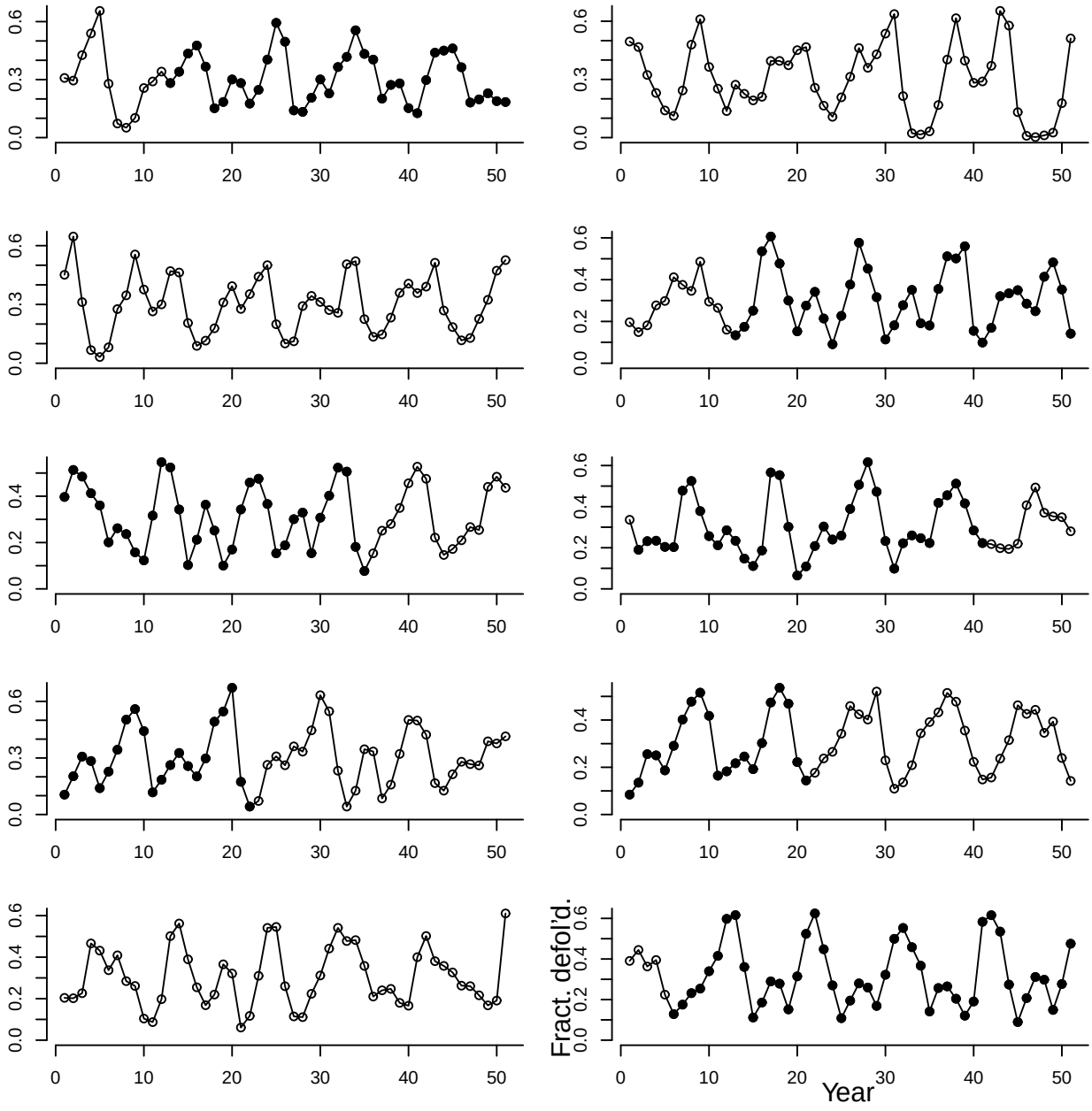


Figure S10: 10 additional realizations of the spatial model, as in fig. S6.

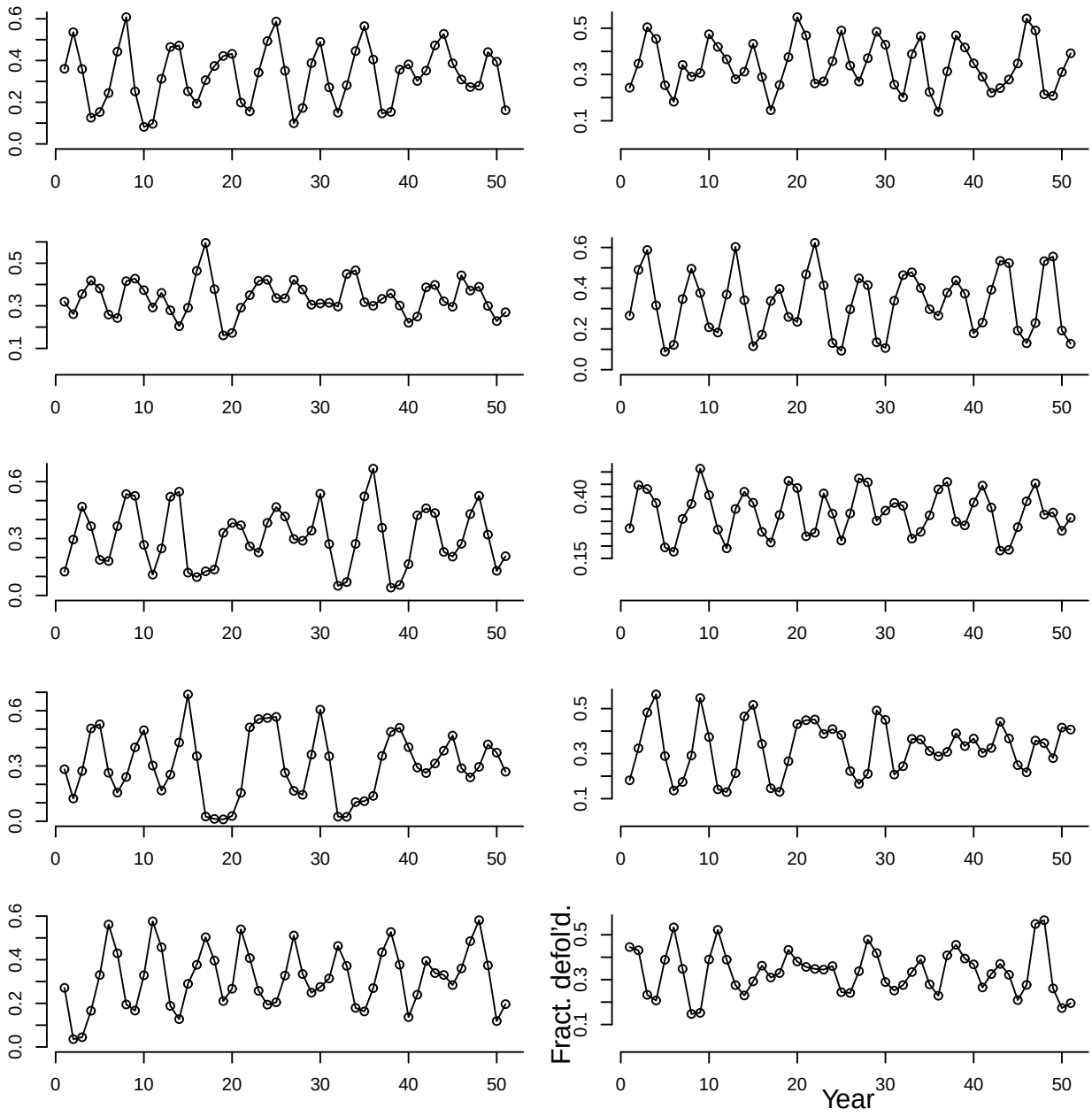


Figure S11: 10 realizations of the spatial model, with 15% of the forest inducible, corresponding to oak-pine forests.

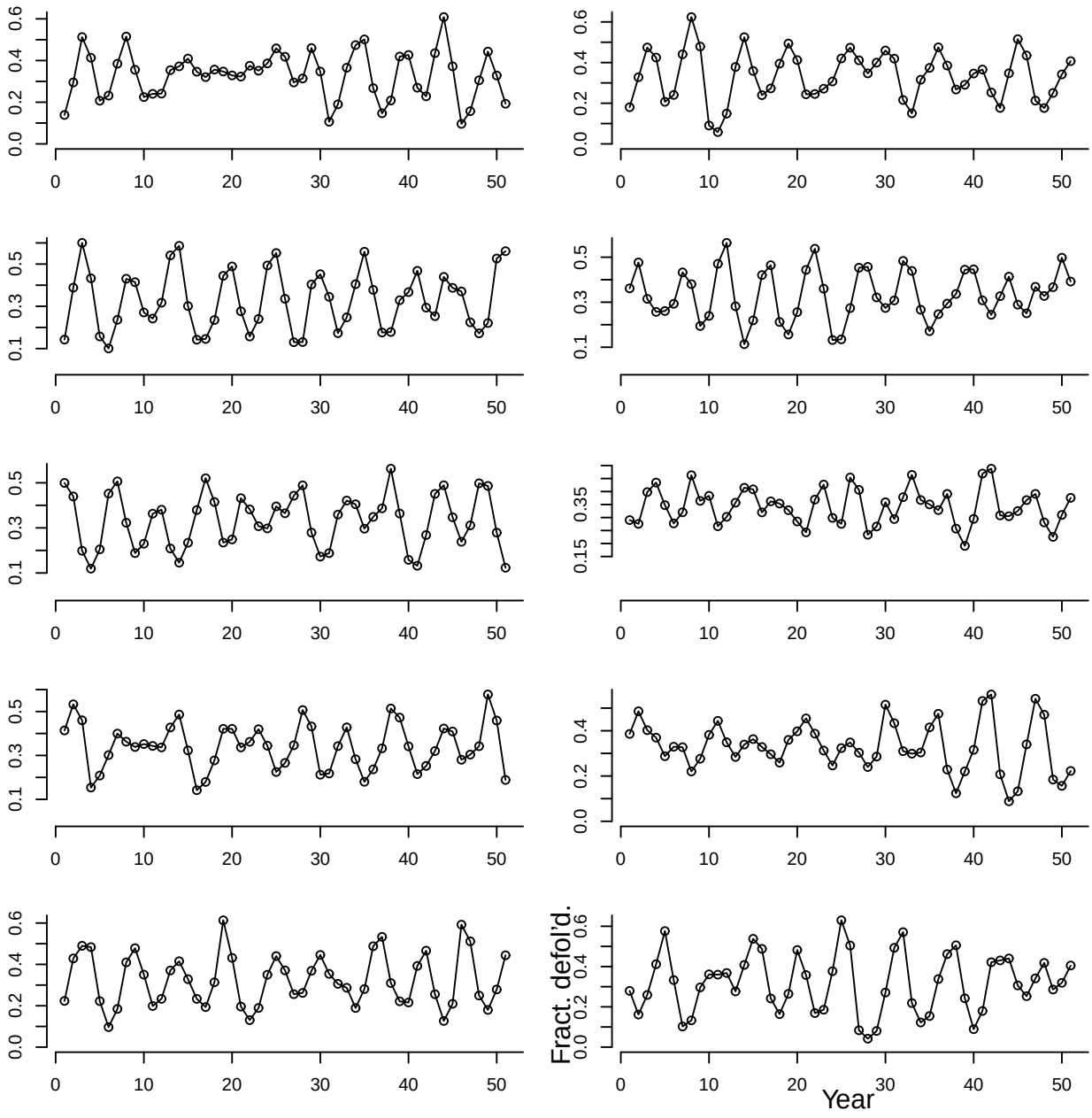


Figure S12: 10 additional realizations of the spatial model, as in fig. S11.

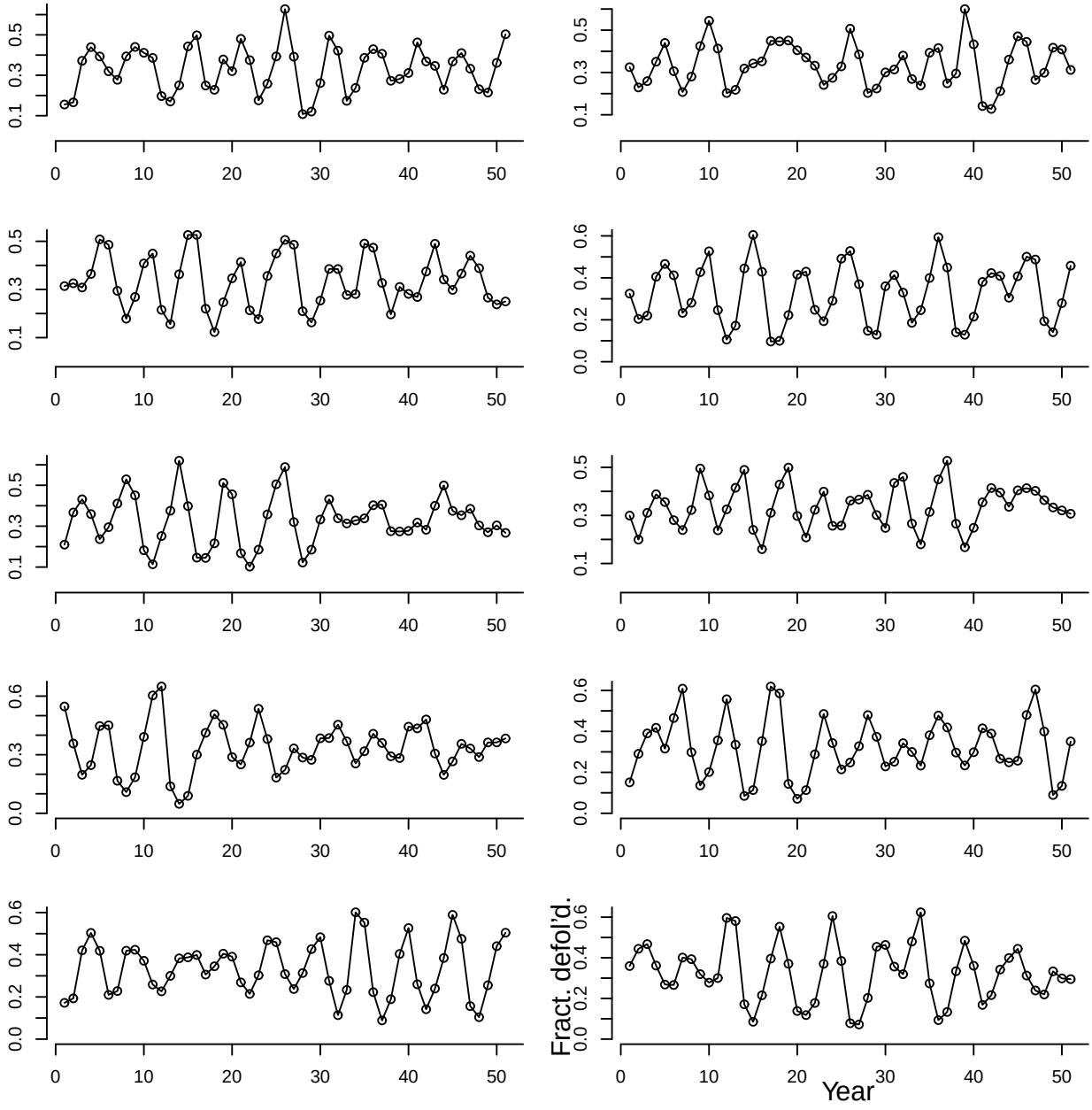


Figure S13: 10 additional realizations of the spatial model, as in fig. S11.

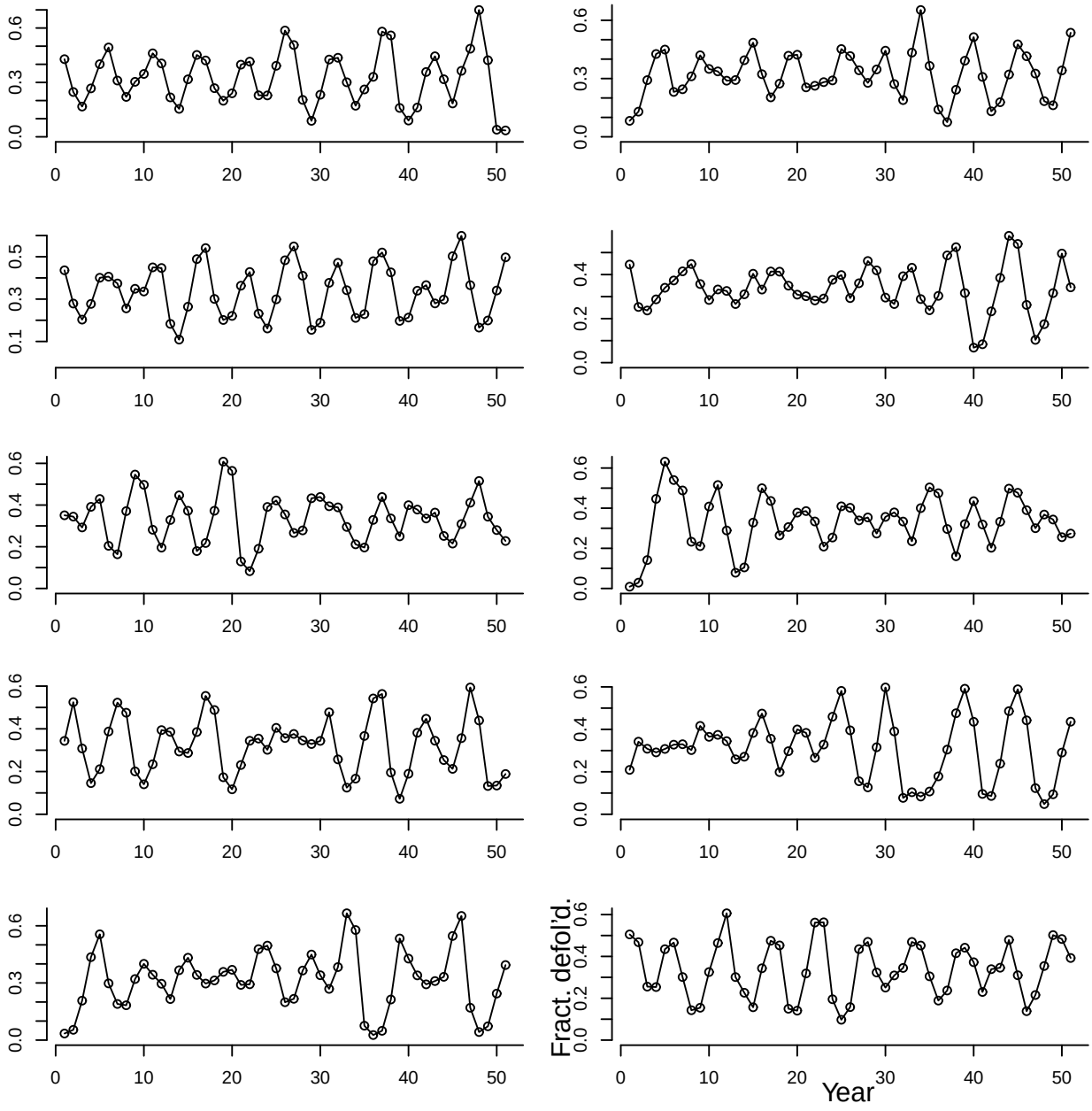


Figure S14: 10 additional realizations of the spatial model, as in fig. S6.

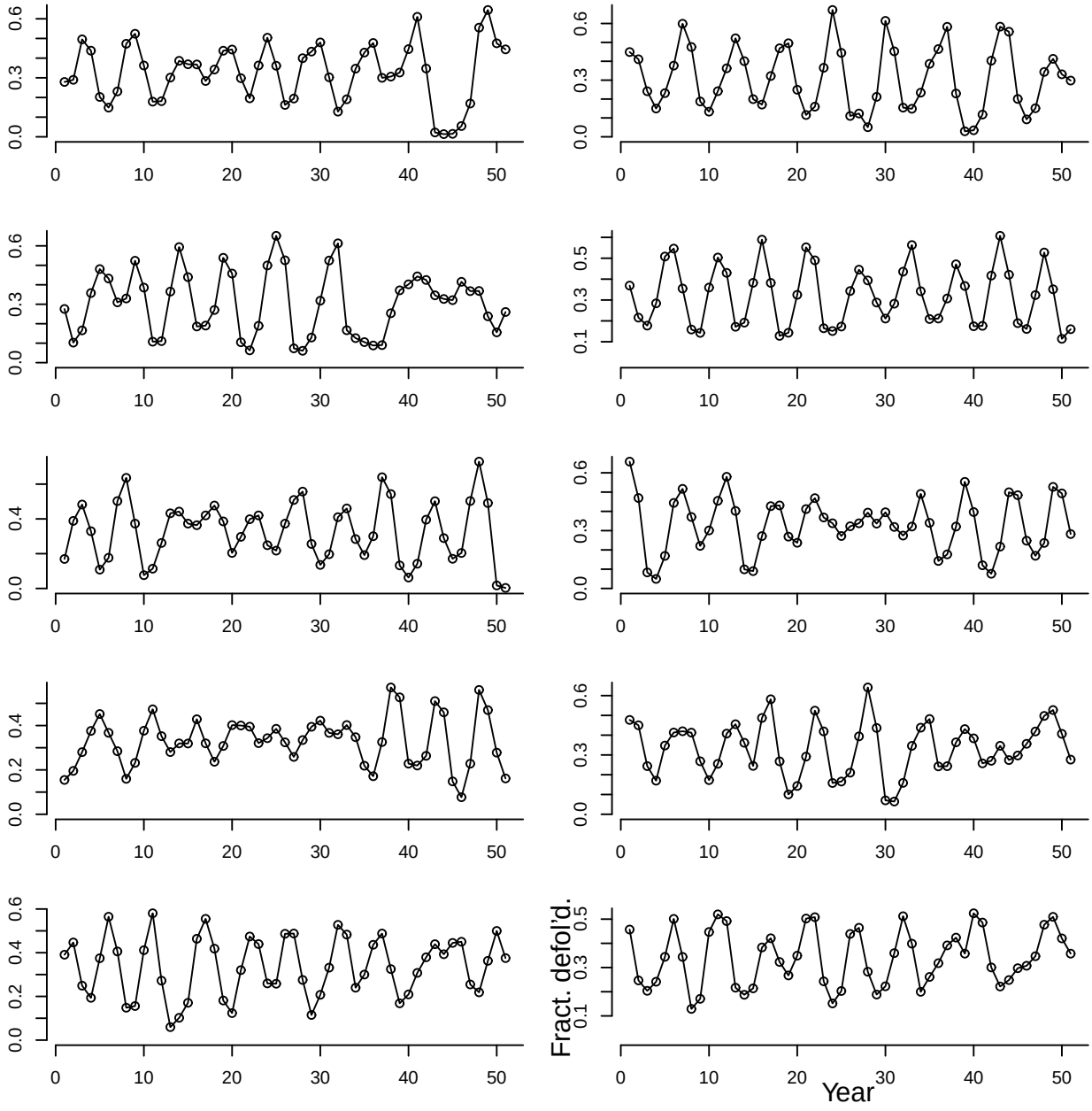


Figure S15: 10 additional realizations of the spatial model, as in fig. S6.

$\hat{\alpha}$ much above the baseline values instead caused the model to do a poor job of fitting the oak-pine data. In short, the model shows realistic output even if the values of $\hat{\alpha}$ are somewhat lower than our best-fit values. We therefore argue that our results are not particularly sensitive to changes in the value of $\hat{\alpha}$.

Increasing $\hat{\alpha}$ also had the effect of increasing the fraction of realizations that produced at least two alternations of mild and severe outbreaks, as in the defoliation data. The effect is modest, however, such that for $\hat{\alpha} = 4$ the fraction was 0.4, instead of the 0.5 produced by $\hat{\alpha} = 8$. The value of $\hat{\alpha}$ on non-induced foliage also had a modest effect on this fraction, such that $\hat{\alpha} = 1$ gives 0.5, $\hat{\alpha} = 0.5$ gives 0.4, and $\hat{\alpha} = 0.25$ gives 0.2. Substantially higher values of $\hat{\alpha}$ on either inducible or non-inducible foliage gave a poor fit to the oak-pine data. A more general point is that, because we fit the values of $\hat{\alpha}$ for the spatial model to the defoliation data, the results of the spatial model are not dependent on the experimental data. This is the basis of our claim in the Discussion that the experimental and observational data provide independent lines of argument.

The reason why individual trajectories in simulated oak-hickory forests do not always match the data has to do with the effects of stochasticity on outbreaks. Weather stochasticity is strongly synchronizing in the model, as it is in nature (Peltonen et al. 2002), but the synchronization is specific to either inducible or non-inducible trees. To illustrate this effect, in fig. S16, we show a realization for which severe and mild outbreaks alternate for the entire time series (upper panel), followed by the associated time series for all spatial locations in the forest plotted on the same axes (lower panel). In this realization of the model, out of the $10^4$ total locations, there were 4329 inducible locations and 5671 non-inducible locations. The time series for the inducible locations are all identical, however, and so they are plotted on top of each other, as are the time series for the non-inducible locations. The effect is that the graph shows only one line for the inducible locations, and one line for the non-inducible locations. The figure thus shows that, on the inducible trees, there was a synchronized cycle with a large amplitude and a period of 9 years, representing the main peak in the power spectrum in the main text, while on the non-inducible trees there was a synchronized cycle with a small amplitude and a period of roughly 4.9 years, representing the sub-harmonic.

The upper panel of fig. S16 thus shows an alternation of mild and severe outbreaks because every other peak of the cycle on non-inducible trees is in near-perfect synchrony with every peak of the cycle on inducible trees. Because of weather stochasticity or stochastic variability in the spatial

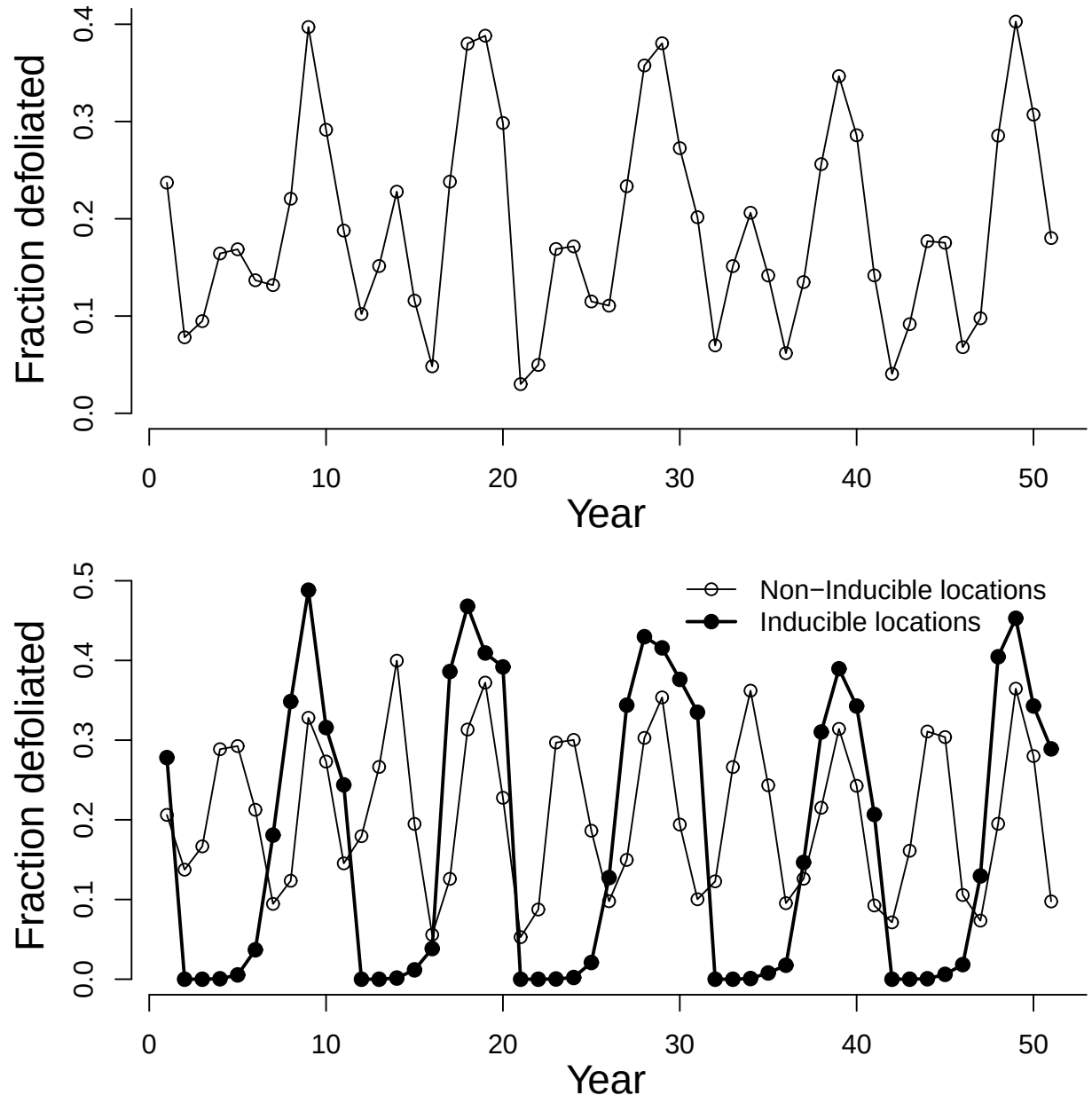


Figure S16: The upper panel shows a single realization of the model, for a case in which the model produces a strict alternation of severe and moderate cycles, as in the defoliation data for oak-hickory forests. The lower panel shows time series for all of the inducible locations and all of the non-inducible locations, such that the data for each location are plotted separately. The lines for the inducible locations are thus all plotted exactly on top of each other, as are the lines for the non-inducible locations. The panel therefore shows that the respective tree types, inducible and non-inducible, have their own synchronized cycles.

locations of inducible and non-inducible trees, in other realizations the peaks of these distinct cycles are not always in synchrony, and in such cases the model trajectory will not show a strict alternation of mild and severe outbreaks. As we mentioned in the main text, the lack of an obvious sub-harmonic in more recent defoliation data may reflect these effects (Johnson et al. 2006), although it may also reflect the effects of the more recently introduced fungal pathogen *Entomophaga maimaiga* (Dwyer et al. 2004). We reiterate, however, that a sub-harmonic never occurs by chance in model trajectories from oak-pine forests because inducible trees represent such a small proportion of oak-pine forests.

### 2.3.2 Modifications of the basic model

In the interests of parsimony, in the main text we present the simplest model that can explain the data, but here we consider alternative model structures, to show that our results are robust to changes in assumptions about the effects of induction. First, in the main text we used a model in which induction affects only variability in transmission, rather than average transmission, because induction had much stronger effects on variability in transmission than it had on average transmission. More generally, however, average transmission is strongly dependent on insect feeding and movement behavior, which are in turn affected by leaf toughness and leaf architecture (Dwyer et al. 2005), whereas variability in transmission is scale-independent and therefore more likely to be robust to differences in leaf characteristics. Because the effects of leaf characteristics on transmission are poorly understood, and because the model that leaves out such effects is more parsimonious, we assumed that differences in host-tree genera only affect variability in transmission. To test whether this assumption affected our conclusions, we also considered a model in which transmission rate declines exponentially with increasing levels of the induced defense, with rate parameter $\eta$, much as variability declines exponentially with defenses in the main model (unlike the corresponding parameter $\psi$ for the change in variability, this parameter cannot be scaled away). We then adjusted $\eta$ to find a value that gave an amplitude of fluctuation of $\log_{10}(\bar{\nu})$ that included the range seen in our experiments ($\eta = 0.1$ gave a good fit to the experimental amplitude of 0.55). As figure (S17) shows, the results are basically the same as for the main model, and in fact the fraction of time series that resemble the time series in the data is even higher (not shown). We repeat, however, that our main model is likely to be more robust, and it also provides a more parsimonious explanation for the defoliation data.

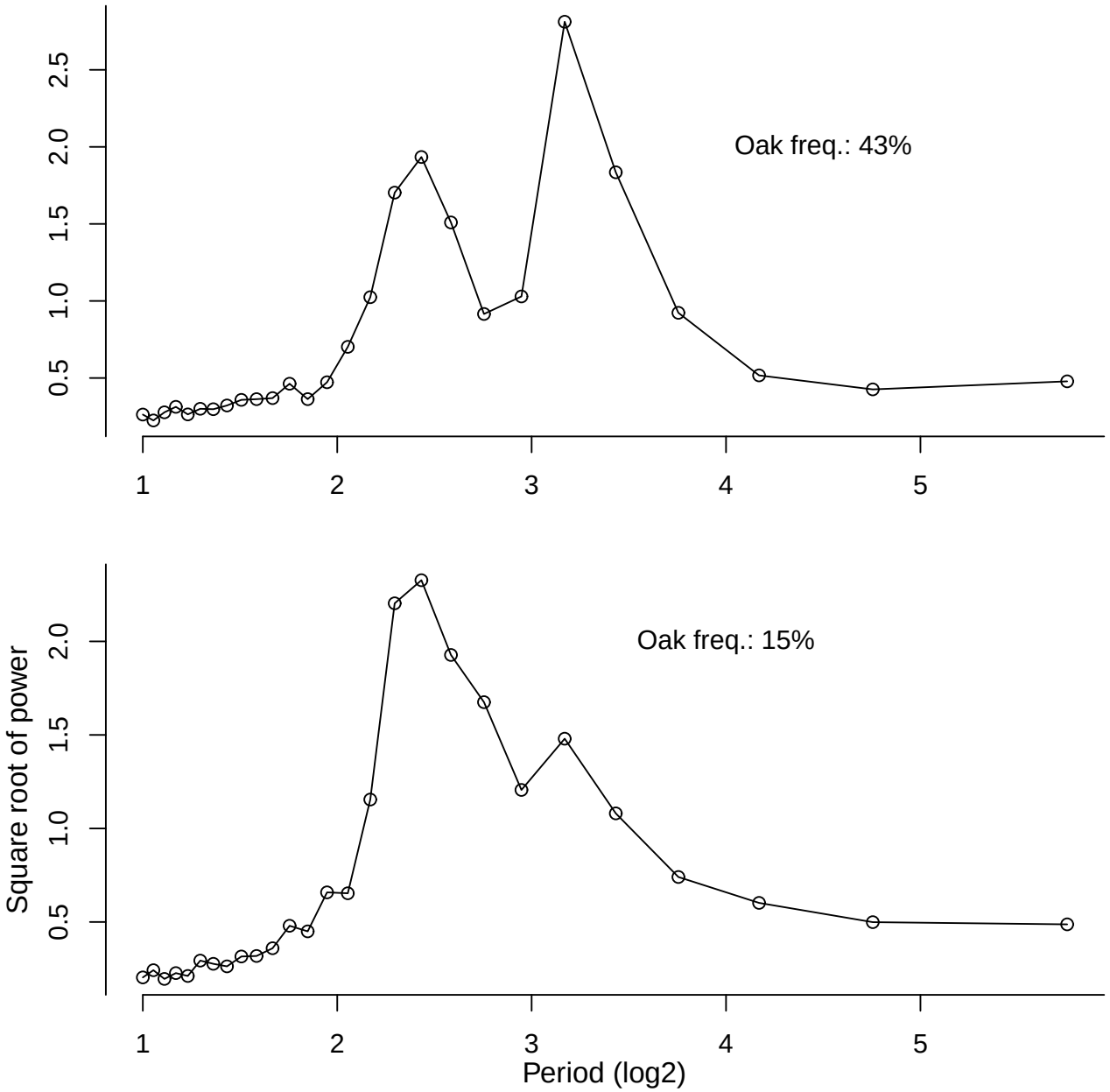


Figure S17: Effects of tannin-dependent average transmission on power spectra of the model output. As in the main text, induced defenses lower variability in infection risk $C$, but in this case they also lower average infection risk $\bar{\nu}$.

As we mentioned in the main text, our basic results are robust to a moderate reduction in the insect's reproductive rate on non-oaks (fig. S18). In this case, the sub-harmonic in the power spec-

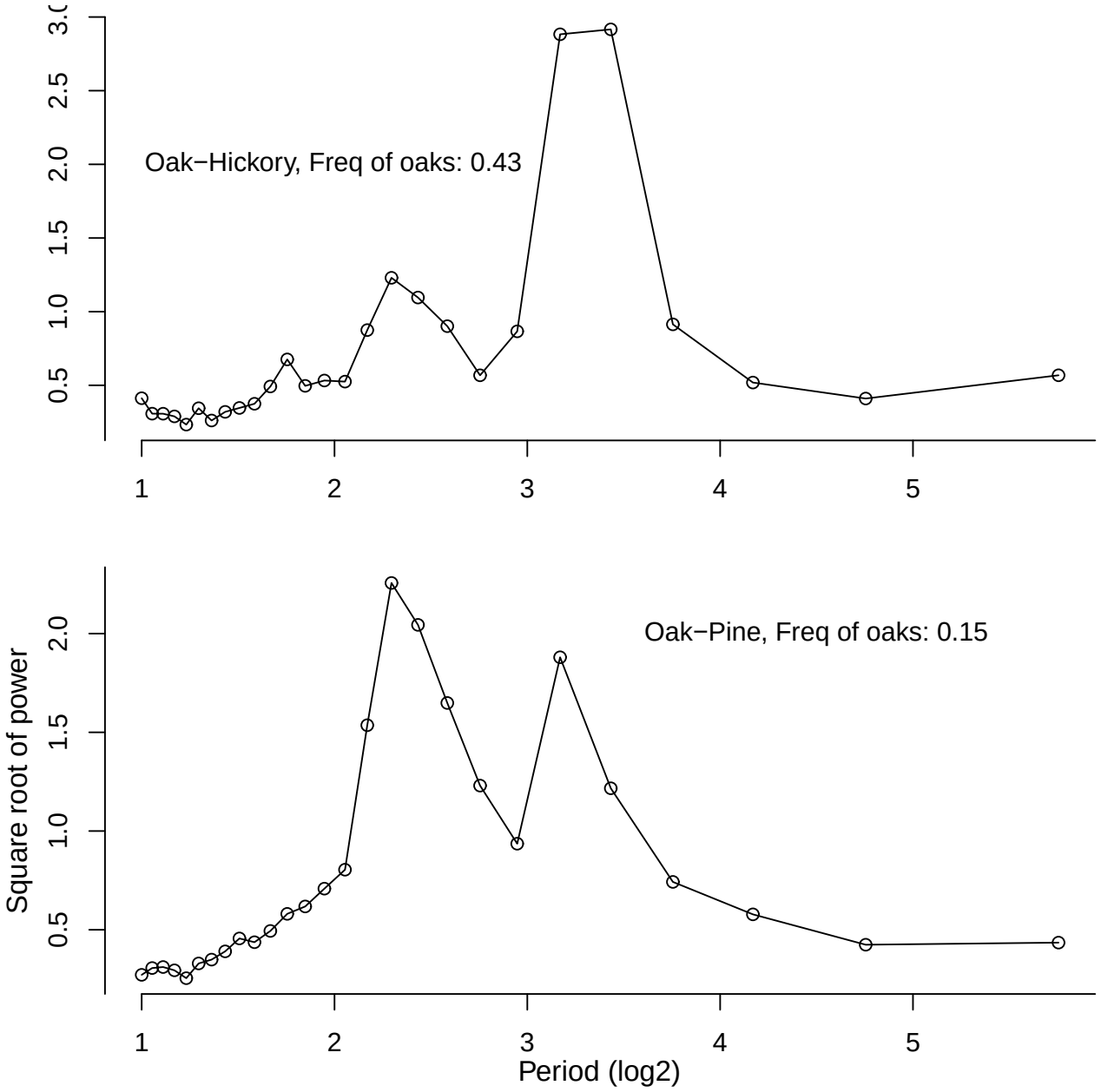


Figure S18: Effects of a 25% reduction in host reproductive rate on non-oak locations on the power spectrum of the defoliation time series. Note that there is an increase in the super-harmonic in oak-pine forests. In spite of the superharmonic, however, the time series of defoliation in oak-pine forests do not show obvious alternation of severe and moderate outbreaks (not shown).

trum in oak-hickory forests is slightly less pronounced than in the power-spectrum in the data (see main text). We also note that, in the figure in the main text, there is a super-harmonic in the model spectrum for the data from oak-pine forests, but it is small enough that we did not emphasize it. We mention it here because fig. S18 shows that lowered reproduction on pines leads to a slightly more pronounced super-harmonic in the spectrum for the model from oak-pine forests, suggesting that the super-harmonic in the data for oak-pine forests may in fact be meaningful.

As we also mentioned in the main text, lowering the reproductive rate on non-oaks alone is not sufficient to produce a sub-harmonic. To see this, we ran the model with low inducibility at all locations, so that the rate of change of the defense $\hat{\alpha} = 1$ everywhere, while again allowing for a lowered insect reproductive rate on non-oaks. As fig. S19 shows, with weak variability in inducibility throughout the forest, there is no sub-harmonic for a range of values of the reduction of host reproductive rate on non-oaks. Variation in inducibility is therefore apparently required for the sub-harmonic.

A related point is that the model predicts that, in oak-hickory forests, there is a shorter-period, lower-amplitude cycle on non-oaks, which in turn implies that gypsy moth densities in oak-hickory forests should be higher on non-oaks in at least some generations (fig. S16). There are no data that permit a direct test of this prediction, but the prediction at least superficially appears to be contradicted by some literature data. Specifically, Lechowicz and Mauffette (1986) reviewed studies of gypsy moth feeding, using data from both choice tests and defoliation surveys to rank different host tree species as "preferred", "acceptable", or "un-acceptable". Based on a range of studies, they ranked oaks as preferred hosts, and hickories and pines as acceptable hosts, implying that hickories and pines should have lower densities of gypsy moths than oaks.

It is important to remember, however, that relative densities on oaks and non-oaks reflect not just the suitability of different tree species as food sources, but also the dynamics of the virus. Indeed, several studies include data in which larval densities are higher on oaks than on non-oaks, but pupal densities a few weeks later are often *lower* on oaks (Lechowicz and Jobin 1983; Mauffette and Lechowicz 1984; Rossiter 1987). Whether these higher pupal densities are translated into higher larval densities in the following generation is unclear, but a high fraction of hatchling larvae do not leave the first foliage they encounter, even if that foliage is not that of a preferred host (Hunter and Lechowicz 1992). Higher pupal densities on non-oaks therefore likely lead to higher initial larval

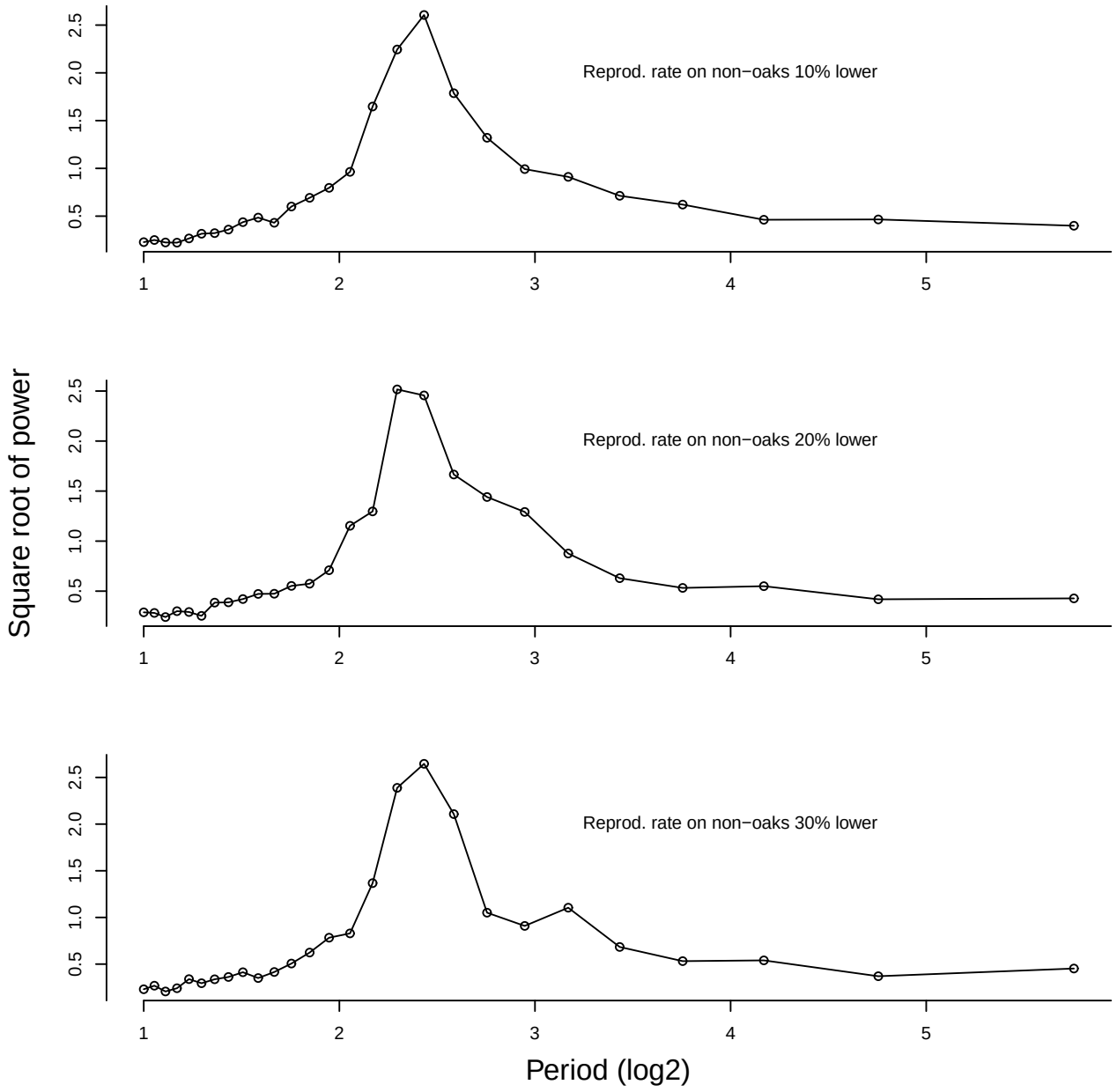


Figure S19: Effects of reductions in host reproductive rate on the power spectrum when there is no variability in inducibility across spatial locations. In all 3 cases, 43% of spatial locations are oaks, corresponding to oak-hickory forests. Irrespective of the reduction in the reproductive rate on non-oaks, there is no meaningful sub-harmonic.

densities on non-oaks in the following generation. The data thus suggest that, at least some of the time, densities on non-oaks are indeed higher than on oaks, as our model predicts. This effect occurs in the model because virus epizootics are more severe on oaks, but an alternative explanation for the pattern in nature is that larvae may move away from oaks near the end of the larval season (Lechowicz and Jobin 1983; Mauffette and Lechowicz 1984; Rossiter 1987). Unfortunately, however, there are no data indicating which explanation is correct.

Moreover, it is not possible to allow for tree-species-specific movement rates in our model, because of a lack of tree-species-specific movement data. Testing whether such movement would alter our model results is therefore also not possible. Our overall argument is thus that, given the available data, our model provides the best explanation for differences in gypsy-moth cycles between forest types.

A final point is that we also tried different numbers of grid points, ranging from a $5 \times 5$ grid to a $250 \times 250$ grid, with the model results presented here based on a $100 \times 100$ grid. As the number of grid points increased beyond $150 \times 150$, realizations that produced exactly alternating high and low defoliation levels became somewhat less likely, although the power spectra were unchanged. This effect suggests that at least mild patchiness in inducibility is necessary for alternating peaks, but the effect is rather weak. Further research is clearly needed to understand such effects.

# References


ABBOTT, K. C. AND DWYER, G. 2008. Using mechanistic models to understand synchrony in forest insect populations: the North American gypsy moth as a case study. American Naturalist 172:613–624.

ANDERSON, R. M. AND MAY, R. M. 1991. Infectious diseases of humans: Dynamics and control. Oxford University Press.

BATE-SMITH, E. C. 1975. Phytochemistry of proanthocyanidins. Phytochemistry 14:1107–1113.

BURDEN, J., NIXON, C., HODGKINSON, A., POSSEE, R., SAIT, S., KING, L., AND HAILS, R. 2003. Covert infections as a mechanism for long-term persistence of baculoviruses. Ecology Letters 6:524–531.

BURNHAM, K. AND ANDERSON, D. 2002. Model selection and multimodel inference: A practical information-theoretic approach. Springer, New York.

CHATFIELD, C. 2003. The Analysis of Time Series. Chapman & Hall, CRC, 6th edition.

COLLETT, D. 2003. Modelling binary data. Chapman & Hall.

D'AMICO, V., ELKINTON, J., DWYER, G., WILLIS, R., AND MONTGOMERY, M. E. 1998. Foliage damage does not affect within-season transmission of an insect virus. Ecology 79:1104–1110.

DOANE, C. 1969. Trans-ovum transmission of a nuclear-polyhedrosis virus in gypsy moth and inducement of virus susceptibility. Journal of Invertebrate Pathology 14:199–210.

DWYER, G. 1991. The roles of density, stage and patchiness in the transmission of an insect virus. Ecology 72:559–574.

DWYER, G., DUSHOFF, J., AND YEE, S. H. 2004. The combined effects of pathogens and predators on insect outbreaks. Nature 430:341–345.

DWYER, G., FIRESTONE, J., AND STEVENS, T. E. 2005. Should models of disease dynamics in herbivorous insects include the effects of variability in host-plant foliage quality? The American Naturalist 165:16–31.

ELDERD, B., DUSHOFF, J., AND DWYER, G. 2008. Does natural selection on disease susceptibility play a role in insect outbreaks? The American Naturalist 172:829–842.

ELKINTON, J. S., HEALY, W. M., BUONACCORSI, J. P., BOETTNER, G. H., HAZZARD, A. M., SMITH, H. R., AND LIEBHOLD, A. M. 1996. Interactions among gypsy moths, white-footed mice, and acorns. Ecology 77:2332–2342.

EVANS, M., HASTINGS, N. A. J., AND PEACOCK, B. 1993. Statistical Distributions, Second Edition. Wiley-Interscience.

FARAWAY, J. 2006. Extending the linear model with R: Generalized linear, mixed effects and nonparametric regression models. Chapman & Hall/CRC.

FULLER, E., ELDERD, B. D., AND DWYER, G. 2012. Pathogen Persistence in the Environment and Insect-Baculovirus Interactions: Disease-Density Thresholds, Epidemic Burnout, and Insect Outbreaks. American Naturalist 179:E70–E96.

GROVE, M. J. AND HOOVER, K. 2007. Intrastadial developmental resistance of third instar gypsy moths (*Lymantria dispar* l.) to *L. dispar* nucleopolyhedrovirus. Biological Control 40:355–361.

HAGERMAN, A. E. AND BUTLER, L. G. 1980. Condensed tannin purification and characterization of tannin-associated proteins. Journal Of Agricultural And Food Chemistry 28:947–952.

HUNTER, A. AND ELKINTON, J. 2000. Effects of synchrony with host plant on populations of a spring-feeding Lepidopteran. Ecology 81:1248–1261.

HUNTER, A. AND LECHOWICZ, M. J. 1992. Foliage quality changes during canopy development of some Northern hardwood trees. Oecologia 89:316–323.

HUNTER, M. D. AND SCHULTZ, J. C. 1993. Induced plant defenses breached - phytochemical induction protects an herbivore from disease. Oecologia 94:195–203.

IL'INYKH, A. AND UL'YANOVA, E. 2005. Latency of baculoviruses. Biology Bulletin 32:496–502.

JOHNSON, D., LIEBHOLD, A., AND BJORNSTAD, O. 2006. Geographical variation in the periodicity of gypsy moth outbreaks. Ecography 29:367–374.

JOHNSON, D. M., LIEBHOLD, A. M., AND BJORNSTAD, O. N. 2005. Circumpolar variation in periodicity and synchrony among gypsy moth populations. Journal of Animal Ecology 74:882–892.

JONES, C., OSTFELD, R., RICHARD, M., SCHAUBER, E., AND WOLFF, J. 1998. Chain reactions linking acorns to gypsy moth outbreaks and Lyme disease risk. Science 279:1023–1026.

KEATING, S. T., MCCARTHY, W. J., AND YENDOL, W. G. 1989. Gypsy moth (*Lymantria dispar*) larval susceptibility to a bacuiovirus affected by selected nutrients, hydrogen ions (pH), and plant allelochemicals in artificial diets. Journal of Invertebrate Pathology 54:165–174.

KENDALL, B. E., BRIGGS, C. J., MURDOCH, W. W., TURCHIN, P., ELLNER, S. P., NISBET, R. M., AND WOOD, S. N. 1999. Why do populations cycle? a synthesis of statistical and mechanistic modeling approaches. Ecology 80:1789–1805.

KOT, M., LEWIS, M., AND VANDENDRIESSCHE, P. 1996. Dispersal data and the spread of invading organisms. Ecology 77:2027–2042.

KUKAN, B. 1999. Vertical transmission of nucleopolyhedrovirus in insects. Journal OF Invertebrate Pathology 74:103–111.

LECHOWICZ, M. AND MAUFFETTE, Y. 1986. Host preferences of the gypsy moth in eastern north american versus european forests. Revue d'entomologie du Quebec 31:43–51.

LECHOWICZ, M. J. AND JOBIN, L. 1983. Estimating the susceptibility of tree species to attack by the gypsy-moth, *Lymantria dispar*. Ecological Entomology 8:171–183.

LIEBHOLD, A. M., HALVERSON, J. A., AND ELMES, G. A. 1992. Gypsy-moth invasion in North America - a quantitative analysis. Journal of Biogeography 19:513–520.

MAUFFETTE, Y. AND LECHOWICZ, M. 1984. Differences in the utilization of tree species as larval hosts and pupation sites by the gypsy-moth, *Lymantria dispar* (Lepidoptera, Lymantriidae). Canadian Entomologist 116:685–690.

MCCULLAGH, P. AND NELDER, J. 1989. Generalized Linear Models. Chapman & Hall, Boca Raton, FL.

MOREAU, G., LUCAROTTI, C. J., KETTELA, E. G., THURSTON, G. S., HOLMES, S., WEAVER, C., LEVIN, D. B., AND MORIN, B. 2005. Aerial application of nucleopolyhedrovirus induces decline in increasing and peaking populations of *Neodiprion abietis*. Biological Control 33:65–73.

MURRAY, K. D. AND ELKINTON, J. S. 1989. Environmental contamination of egg masses as a major component of transgenerational transmission of gypsy-moth nuclear polyhedrosis-virus (LdMNPV). Journal Of Invertebrate Pathology 53:324–334.

MYERS, J., MALAKAR, R., AND CORY, J. 2000. Sublethal nucleopolyhedrovirus infection effects on female pupal weight, egg mass size, and vertical transmission in gypsy moth (Lepidoptera : Lymantriidae). Environmental Entomology 29:1268–1272.

PELTONEN, M., LIEBHOLD, A. M., BJORNSTAD, O. N., AND WILLIAMS, D. W. 2002. Spatial synchrony in forest insect outbreaks: roles of regional stochasticity and dispersal. Ecology 83:3120–3129.

PINHEIRO, J. C. AND BATES, D. M. 2004. Mixed-effects models in S and S-PLUS. Springer, New York, New York.

PODGWAITE, J. D., SHIELDS, K. S., ZERILLO, R. T., AND BRUEN, R. B. 1979. Environmental Persistence of the Nucleopolyhedrosis Virus of the Gypsy Moth, *Lymantria dispar*. Environmental Entomology 8.

R DEVELOPMENT CORE TEAM 2009. R: A language and environment for statistical computing. R Foundation for Statistical Computing, Vienna, Austria.

RENSHAW, E. 1993. Modelling Biological Populations in Space and Time. Cambridge University Press.

ROSS, S. M. 1984. A first course in probability. Macmillan.

ROSSITER, M. C. 1987. Use of a secondary host by non-outbreak populations of the gypsy moth. Ecology 68:857–868.

SCHULTZ, J. AND BALDWIN, I. T. 1982. Oak leaf quality declines in response to defoliation by gypsy moth larvae. Science 217:149–150.

WATANABE, H. 1987. The host population, pp. 71–112. In J. Fuxa and Y. Tanada (eds.), Epizootiology of insect diseases. Wiley: New York.

WILLIAMS, D., FUESTER, R., METTERHOUSE, W., BALAAM, R., BULLOCK, R., AND RJ, C. 1991. Oak defoliation and population-density relationships for the gypsy-moth (Lepidoptera:Lymantriidae). Journal of Economic Entomology 84:1508–1514.

WOODS, S. A. AND ELKINTON, J. S. 1987. Bimodal patterns of mortality from nuclear polyhedrosis-virus in gypsy-moth (*Lymantria-dispar*) populations. Journal Of Invertebrate Pathology 50:151–157.